12-2015

Heat transfer mechanisms in water-based nanofluids.

Masoudeh Ahmadi
University of Louisville

HEAT TRANSFER MECHANISMS IN WATER-BASED NANOFLUIDS

By

Masoudeh Ahmadi
M.S., Tehran Azad University, 2010

A Dissertation
Submitted to the Faculty of the
J.B. Speed School of Engineering of the University of Louisville
in Partial Fulfillment of the Requirements
for the Degree of

Doctor of Philosophy in Chemical Engineering

Department of Chemical Engineering
University of Louisville
Louisville, KY 40292

December 2015

HEAT TRANSFER MECHANISMS IN WATER-BASED NANOFLUIDS

By

Masoudeh Ahmadi
M.S., Tehran Azad University, 2010

A Dissertation Approved on

20 November 2015

by the following Dissertation Committee:

_____
Gerold A. Willing (Dissertation Director)

_____
James C. Watters

_____
Eric Berson

_____
Gail Depuy

DEDICATION

This Dissertation is dedicated to my lovely parents

Mr. Ali Ahmadi
And
Mrs. Batool Mahmoodi

Who have given me invaluable educational opportunities and make me who I am

And my beloved husband

Mr. Farshad Farid

Who has always supported me in this process.

ACKNOWLEDGMENTS

I would like to express my deepest gratitude to my Ph.D advisor, Prof. Gerold A. Willing for his guidance and support during my Ph.D study at University of Louisville. Dr. Willing provided an exciting and relaxing working environment and great opportunities to develop new ideas. It was a very enjoyable time working in his research group.

I would like to thank Prof. James C. Watters, Prof. Eric Berson and Prof. Gail W. Depuy for agreeing to be my dissertation committee.

Finally, I would like to thank my family for their encouragement and support, without which this dissertation and research would not have been possible.

ABSTRACT

HEAT TRANSFER MECHANISMS IN WATER-BASED NANOFLUIDS

Masoudeh Ahmadi

20 November 2015

Nanofluids are a class of heat transport fluids created by suspending nano-scaled metallic or nonmetallic particles into a base fluid. Some experimental investigations have revealed that the nanofluids have remarkably higher thermal conductivities than those of conventional pure fluids and are more suited for practical application than the existing techniques of heat transfer enhancement using millimeter and/or micrometer-sized particles in fluids. Use of nanoparticles reduces pressure drop, system wear, and overall mass of the system leading to a reduction in costs over existing enhancement techniques.

In this work, the heat transfer coefficient is determined experimentally using copper oxide (CuO) based nanofluids. CuO nanoparticles (40nm) with different particles loadings (0%, 0.25%, 1% and 2% by weight) were dispersed into water without use of an additional dispersant. The heat transfer coefficient for each nanofluid was measured at specific flow rates and initial fluid temperatures through a high thermal conductivity

copper tube with a constant heat flux supplied at the wall. The experimental results revealed that the heat transfer coefficient for each nanofluid increased with increasing Reynolds Number (Re) which is not unexpected in cases of convective heat transfer. Under conditions of constant particle loading and Re, the heat transfer coefficient was generally observed to increase with decreasing inlet nanofluid temperature.

Since the generally observed trends were similar for all nanofluids under all conditions, the effectiveness of CuO nanoparticles in improving heat transfer coefficient relative to the heat transfer coefficient of the base was determined. This so called heat transfer enhancement is defined as the ratio of the heat transfer coefficient of the nanofluid and that of the base fluid. The goal of this investigation was to specifically determine the role of nanoparticles in the enhancement of the overall heat transfer coefficient of a nanofluid. Unfortunately, the variation of the heat transfer coefficient enhancement with respect to changes in nanoparticle concentration and Re is not consistent across the initial temperatures investigated. This variation was especially clear under laminar flow conditions where at 40°C the 0.25%wt gives the highest heat transfer coefficient enhancement while at 70°C it is the 1.0%wt that gives the highest enhancement.

In an effort to understand the nature of these seemingly unpredictable variations, we developed a Computational Fluid Dynamics (CFD) model using an Eulerian-Lagrangian approach to study the nature of both the laminar and turbulent flow fields of the fluid phase as well as the kinematic and dynamic motion of the dispersed nanoparticles. The goal was to provide additional information about dynamics of both the fluid and particles to explain the experimentally observed trends of the heat transfer coefficient

enhancement of CuO nanofluids relative to both nanoparticle concentrations and fluid flow conditions. The simulation results indicate that heat transfer enhancement significantly depends on particle motion relative to the tube wall and the thermal boundary layer. This is especially true in the case of laminar flow where heat transfer enhancement can only occur in cases where the nanoparticles can move beyond the thermal boundary layer and into the bulk flow of the fluid.

TABLE OF CONTENTS

LIST OF TABLES

TABLE PAGE

LIST OF FIGURES

FIGURE PAGE

CHAPTER I

INTRODUCTION

1.1 Nanotechnology History

The first use of the concepts found in 'nano-technology' was in "There's Plenty of Room at the Bottom", a talk given by physicist Richard Feynman at an American Physical Society meeting at California Institute of Technology (Caltech) on December 29, 1959 [1]. Feynman described a process by which the ability to manipulate individual atoms and molecules might be developed, using one set of precise tools to build and operate another proportionally smaller set, and so on down to the needed scale. Feynman noted that scaling issues would arise from the changing magnitude of various physical phenomena: gravity would become less important while the surface tension and van der Waals attraction would become increasingly more significant.

The term "nanotechnology" was first defined by Norio Taniguchi of the Tokyo Science University in a 1974 paper [2]. Norio mentioned that "'Nano-technology' mainly consists of the processing of, separation, consolidation, and deformation of materials by one atom or one molecule." Since that time the definition of nanotechnology has been extended to include features as large as 100 nm. In addition, the idea that nanotechnology

embraces structures exhibiting quantum mechanical aspects, such as quantum dots, has further evolved its definition. Dr. Tuomo Suntola and co-workers in 1974 developed and patented the process of atomic layer deposition, for depositing uniform thin films one atomic layer at a time. In the 1980s, Dr. K. Eric Drexler explored the idea of nanotechnology as a deterministic, rather than stochastic, handling of individual atoms and molecules. His vision of nanotechnology is often called "Molecular Nanotechnology" (MNT) or "molecular manufacturing."

Nanotechnology is the manipulation of matter with at least one dimension sized from 1 to 100 nanometers. Nanotechnology involves imaging, measuring, modeling, and manipulating matter at this length scale. Dimensions between 1 and 100 nanometers are known as the nanoscale. At the nanoscale, physical, chemical, and biological properties may be different in important ways from the properties of bulk materials and single atoms or molecules, which leads to better performance of the materials in nanscale.

Nanotechnology is helping to significantly improve many technology and industry sectors such as: information technology, energy, environmental science, medicine, homeland security, food safety, and transportation, among many others. Nanotechnology can be used to collect and store energy, reinforce materials, sense contaminants, enable life-saving drugs, and shrink and accelerate computational devices in both incremental and paradigm-shifting ways. Moreover, nanotechnology has enabled development of entirely new materials and devices that can be exploited in each of these and countless other applications [3].

In 2001 NNI (National Nanotechnology Initiative) was launched with eight agencies. The NNI today consists of the individual and cooperative nanotechnology-related

activities of 25 Federal agencies with a range of research and regulatory roles and responsibilities. The NNI agencies invest at various industries, such as chemistry, engineering, biology, materials science, and physics. The interest in nanotechnology arises from its high potential to impact numerous fields as mentioned before. One of the most important research areas in this plan is the study and application of fundamental nanoscale phenomena and processes.

1.2 Nanofluid History

The concept of nanofluids as coined by researchers at Argonne National Laboratory in 1995 refers to a new class of potential heat transport fluids created by suspending nano-scaled metallic or nonmetallic particles into a base fluid [4]. Some experimental studies have revealed that the nanofluids have remarkably higher thermal conductivities than those of conventional pure fluids and have great potential for heat transfer enhancement. Nanofluids are more suited for practical application than existing techniques for enhancing heat transfer by adding millimeter and/or micrometer-sized particles in fluids since nanofluids incur little or no penalty in pressure drop because the nanoparticles are so small (usually less than 100nm) that they behave like a pure fluids without any particles in it. In addition, nanoparticles are less likely to cause wear because of their small sizes [5-7].

Some devices such as high speed microprocessors, laser application apparatus, super conducting magnets and opto-electronics require high heat transfer cooling systems [8]. With increasing heat transfer rates required by existing heat exchange equipment, conventional process fluids with low thermal conductivities can no longer meet the

requirements of high intensity heat transfer. Low thermal property of heat transfer fluids is a primary limitation to development of high compactness and effectiveness of heat exchangers. Many techniques have been proposed to enhance the heat transfer in these types of equipment. An effective way of improving the thermal conductivity of fluids is to suspend small solid particles in the fluids. Since the thermal conductivity of most solids is significantly greater than that of fluids, it is expected that adding nanoparticles to the heat transfer fluids will significantly improve their thermal performance. Traditionally, solid particles of micrometer or millimeter magnitudes were mixed in the base liquid. Although the solid additives may improve the heat transfer coefficient, practical uses are limited as the micrometer or millimeter sized particles settle rapidly, clog flow channels, erode pipelines and cause pressure drops [5]. Industrially, this technique is not attractive because of these inherent problems.

These problems can be overcome with the use of nanofluids, which are a dispersion of nanosized particles in a base fluid. Nanofluids are a class of heat transfer fluids that have many advantages. They have better stability compared to those fluids containing micro- or milli-sized particles, moreover, they have higher thermal transfer capability than their base fluids. Such advantages offer important benefits for numerous applications in many fields such as transportation, heat exchangers, electronics cooling, nuclear systems cooling, biomedicine and food of many types. For example, in cooling systems, a 50/50 ethylene glycol (EG) and water mixture is commonly used as an automotive coolant. The mixture is a relatively poor heat transfer fluid compared to pure water. Water/EG mixtures with additional nanoparticles are currently being studied to enhance heat transfer performance [9]. Nanoparticles can improve the heat transfer coefficient of pure ethylene glycol.

Therefore, the resulting nanofluid performs better at low pressure working conditions and smaller coolant system size when compared to the 50/50 mixture. Finally, smaller and lighter radiators can be used to increase engine performance and fuel efficiency. Large companies like GM and Ford all have ongoing nanofluid research projects for this very reason. Nanofluids can also be used as the working fluid for heat pipes in electronic cooling applications. Nanofluids can significantly reduce the thermal resistance of the heat pipe when compared to conventional deionized water. In the biomedical field, iron-based nanoparticles could be used as a delivery vehicles for drugs or radiation without damaging nearby tissue to circumvent side effects of traditional cancer treatment methods. Such particles could be guided in the bloodstream to a tumor using magnets external to the body [10]. Advances in thermal management will significantly impact the cost, overall design, reliability and performance of the next generation of several engineering applications [11].

Nowadays, nanofluids are considered to be the next-generation heat transfer fluids as they offer exciting new possibilities to enhance heat transfer performance compared to pure liquids. They have superior properties compared to conventional heat transfer fluids, as well as fluids containing micro-sized metallic particles [12]. Large enhancement of heat transfer performance has been relative to the small amount of material added to the system. The main reasons that contributed to this enhancement of heat transfer performance are [13]:

a) The suspended nanoparticles increase the surface area for heat transfer and the heat capacity of the fluid.
b) The suspended nanoparticles increase the effective thermal conductivity of the fluid.

c) The interaction and collision among particles, fluid and the flow passage surface are intensified.

d) The mixing fluctuation and turbulence of the fluid are intensified.

e) The dispersion of nanoparticles flattens the transverse temperature gradient of the fluid.

Many researchers have considered using nanofluids in heat exchange systems to replace conventional thermal working fluids such as water, ethylene glycol (EG) and engine oil. Substantially increased thermal conductivities of nanoparticle suspensions containing a small amount of metal such as, Cu, or nonmetals like SiC, Al_2O_3, and CuO nanoparticles have been reported recently because they have higher thermal conductivity compared to the conventional thermal fluids [14]. In general, the results indicate that the heat transfer coefficient increased by adding nanoparticles to the conventional fluid [8,15,16]. Figure 1.1 illustrates the thermal conductivities of different metals and fluids. It can be concluded from here that metals with their higher thermal conductivity when compared to the conventional fluids could lead to increases in the overall heat transfer coefficient when added to the conventional fluids.

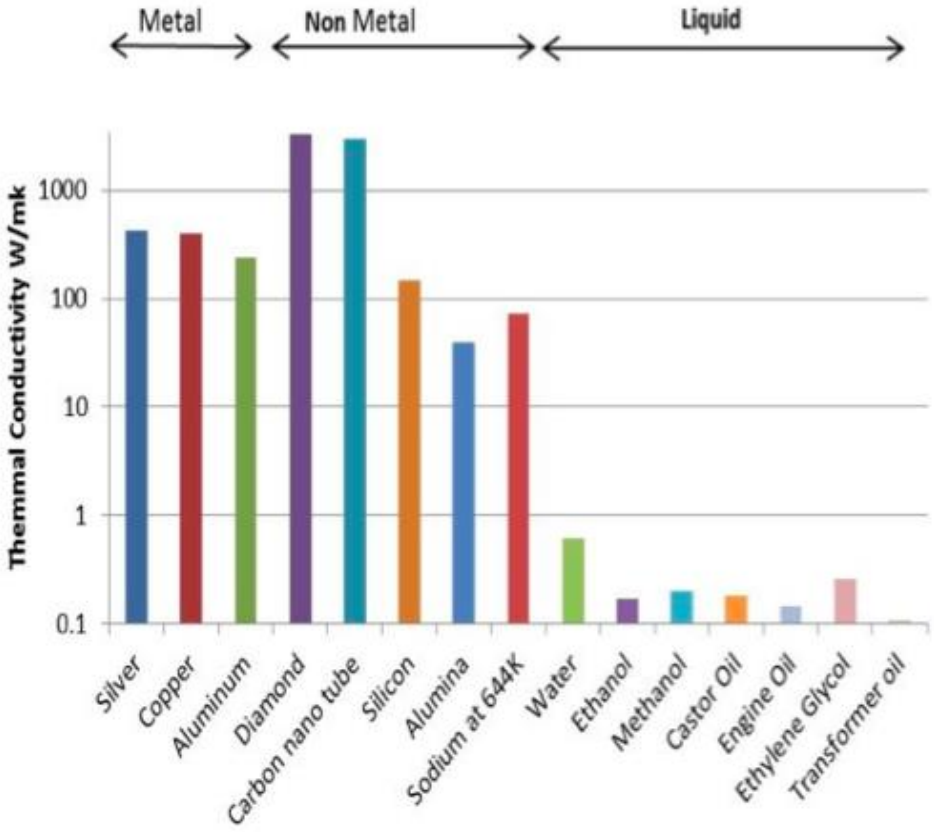

Figure 1.1Thermal conductivity of metals, nonmetal and liquids

Numerous research works about thermal performance of nanofluids have been published on experimental or theoretical evaluation in recent decades. It can be seen from Figure 1.2 that there have been a total of 990 published research nanofluids from 2001 to 2010 [17]. Different particle sizes, shapes and volume fractions have been studied by research groups [13, 18, 19]. Most studies have focused on the enhancement of the thermal conductivity of nanofluids whereas the studies on the enhancement of the heat transfer coefficient have been limited and mostly focused on carbon based nanoparticles. Due to inconsistencies within the research conclusions of these works, nanofluid research work is still under heavy investigation. Some references related to the current experimentation are reviewed in the following paragraphs.

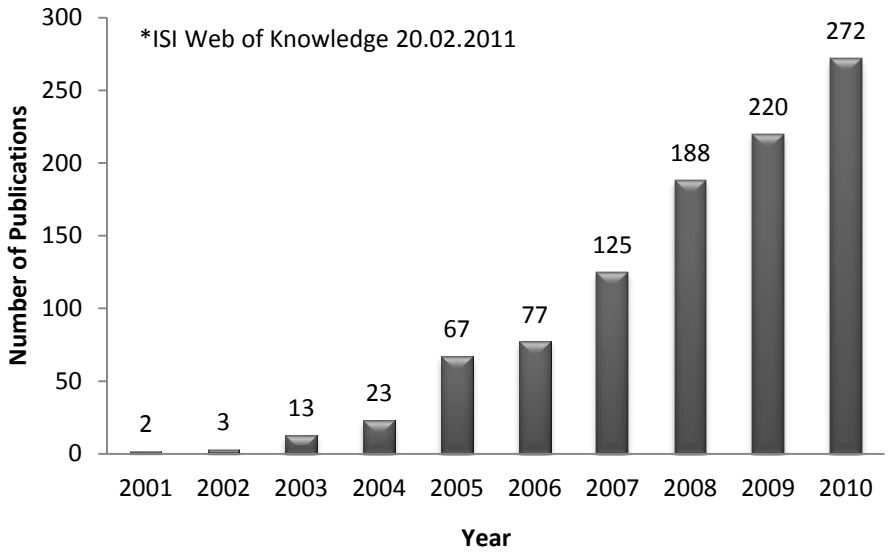

Figure 1.2 Number of published research articles on nanofluids between 2000 and 2010

1.3 Experimental Research on Thermal Conductivity of Nanofluids

One of the most studied areas of nanofluid for heat transfer purposes is the enhancement of thermal conductivity and a big portion of these studies have focused on automotive applications of nanofluids. The impact of various parameters on the enhancement of thermal conductivity of nanofluids has been studied. These parameters are particle size, particle concentration, particle material, base fluid material, and operating temperature.

Lee et al. [7], Wang et al. [6] and Xie et al. [20] have studied the effect of particle size on thermal conductivity. They have measured the enhancement of thermal conductivity using Al_2O_3 nanoparticles with sizes of 28nm, 38nm and 60nm, respectively dispersed in water. For spherical nanoparticles. The enhancement ratio increased with increasing

volume concentration of nanoparticles. The larger 60nm particles showed the highest enhancement. Interestingly though, it was the 38nm particle that showed the least enhancement and not the smaller particle of 28nm. Because of this, no clear conclusions can be made from the results. Similar comparisons can be made from the work of three groups' where different sizes of Al_2O_3 nanoparticles dispersed in ethylene glycol were studied. This time, the intermediate-sized particle of 28nm exhibited the best enhancement.

Most research groups have studied the effect of volume concentration of nanofluids on the enhancement of thermal conductivity [7, 20-27]. Certain type of nanoparticle with different concentrations up to 5% were used to make nanofluids and the thermal conductivity was measured. Particle size or base fluid material may vary but the general trend in all cases was that thermal conductivity enhancement increases with increased particle volume concentration or weight fraction.

The effect of particle material on the enhancement of thermal conductivity is hard to find since different research groups used different sizes of nanoparticles and conducted experiments under different conditions. It can be concluded from the results from Wang et al. [6] (28nm Al_2O_3/water, 23nm CuO/water), Lee et al. [7] (24nm CuO/water), Das et al. [24] (29nm CuO/water), and Xie et al. [28] (26nm SiC/water) that particle material has little effect on the enhancement for those relatively low thermal conductivity particles. Similar results were found for ethylene glycol (EG) based nanofluids by comparing the data from Xie et al. [28, 20] (26nm Al_2O_3/EG, 26nm SiC/EG), Wang et al. [6] (28nm Al_2O_3/EG), Lee et al. [7] (24nm CuO/EG).

Water and ethylene glycol are the two most commonly used base fluids. Xie and

colleagues [29] measured the enhancement of thermal conductivity by using 60nm Al_2O_3 dispersed in these two base fluids and oil. Results showed increased thermal conductivity enhancement for heat transfer fluids with lower thermal conductivity. Water is the best heat transfer fluid with the highest thermal conductivity of the fluids compared. But it showed the least enhancement around 10%-23%, while Al_2O_3/oil nanofluid showed a maximum enhancement of 38%. Although this trend was not supported by results from all research groups, generally it was the case. This result is encouraging because heat transfer enhancement if often most needed when poorer heat transfer fluid are involved. Table 1.1 shows all the research discussed above. Types of nanofluids and testing parameters are listed with enhancement ratio obtained.

Table 1.1 Thermal conductivity enhancements

Author/Year	Nanofluid	Particle size (nm)	Concentration (vol%)	Enhancement ratio
Lee et al./1999[7]	Al_2O_3/water	38.4	1.00 – 4.30	1.03 – 1.10
	CuO/water	23.6	1.00 – 3.41	1.03 – 1.12
	Al_2O_3/ethylene glycol	38.4	1.00 – 5.00	1.03 – 1.18
	CuO/ethylene glycol	23.6	1.00 – 4.00	1.05 – 1.23
Wang et al./1999[6]	Al_2O_3/water	28	0.19 – 1.59	1.01 – 1.10
	CuO/water	23		
	Al_2O_3/ethylene glycol	28	5.00 – 8.00	1.25 – 1.41
	CuO/ethylene glycol	23	6.20 – 14.80	1.24 – 1.54
	Al_2O_3/engine oil	28	2.25 – 7.40	1.05 – 1.30
	Al_2O_3/pump oil	28	5.00 -7.10	1.13 – 1.20
Xie et al./2002[28]	SiC/water	26 sphere	0.78 – 4.18	1.03 – 1.17
		600 cylinder	1.00 – 4.00	1.06 – 1.24
	SiC/ethylene glycol	26 sphere	0.89 – 3.50	1.04 – 1.13
		600 cylinder	1.00 – 4.00	1.06 – 1.23
Xie et al./2002[29]	Al_2O_3/water	60.4	5.00	1.23
	Al_2O_3ethylene glycol	60.4	5.00	1.29
	Al_2O_3/pump oil	60.4	5.00	1.38
Das et al./2003[24]	CuO/water			
	(21°C)	28.6	1.00 – 4.00	1.07 – 1.14
	(36°C)	28.6	1.00 – 4.00	1.22 – 1.26
	(51°C)	28.6	1.00 – 4.00	1.29 – 1.36

Effect of temperature on thermal conductivity was also studied. In general, temperature affects thermal conductivity remarkably. Therefore, the thermal conductivity enhancement of nanofluids is also temperature-sensitive. Das et al. [24] used nanofluids based on 38nm Al_2O_3 dispersed in water to measure thermal conductivity under three different temperatures at 21°C, 36°C and 51°C. Results indicated that enhancement

increased as temperature was increased. A similar trend was observed by many other research groups [30-33] except Masuda et al. [23] who concluded that enhancement of thermal conductivity decreased with increased temperature. This trend is also important for engineering applications where most fluids operate at elevated temperatures.

Although thermal conductivity is very important, it is more critical to know heat transfer coefficient for the convective flow systems. In the next section we will discuss heat transfer coefficient and the experiments research on heat transfer coefficient.

1.4 Experimental Research on Heat Transfer Coefficient Enhancement

The heat transfer coefficient, the proportionality constant between the heat flux and the thermodynamic driving force for the flow of heat, shows how effectively heat can be transferred within a system. The heat transfer coefficient of a nanofluid is more important than the thermal conductivity as this determines how effectively the heat can be transferred within a system under flow conditions. The heat transfer coefficient can be passively enhanced by changing flow geometry, system parameters (temperature, velocity, ect), or by enhancing the thermal conductivity of the fluid. In most existing systems, the first two of these are set by design, which leaves enhancement of the heat transfer properties of the fluid as the only method to enhance heat transfer within the system.

If nanofluids can improve the heat transfer coefficient, they can lead to increased energy and fuel efficiencies, lower pollution, and improved reliability. To this end, it is essential to directly measure the heat transfer performance of nanofluids under flow

conditions typical of specific applications. While not as common as reports on the enhancement of thermal conductivity in nanofluids, there are still several significant studies on the enhancement of the heat transfer coefficient under flow conditions. It should be noted that most heat transfer studies were presented using Nusselt number *Nu*, which is the ratio of convective to conductive heat transfer across the boundary. It is defined as:

$$Nu = \frac{h \cdot D}{k} \tag{1.1}$$

where h is the heat transfer coefficient, D is the diameter of the tube, and k is thermal conductivity of the fluid.

There has been a large number of works in Al_2O_3 /water due to high availability of alumina in different sizes. Wen and Ding have studied Al_2O_3/water nanofluids in laminar flow (Reynolds number range from 700 to 1950) under constant wall heat flux and indicated that the convective heat transfer coefficient of a nanofluid ncreases with Reynolds number and nanoparticle concentration, but the influence of the Reynolds number was not as significant as the effect of nanoparticle concentration [21]. Nguyen et al reported on the heat transfer coefficient of Al_2O_3/water nanofluids flowing through a microprocessor liquid cooling system under turbulent flow conditions. They reported that the heat transfer coefficient of the nanofluid is higher that than of the base fluid. They also found that the nanofluid with 36nm diameter particles gave a higher heat transfer coefficient than the nanofluid with a 47nm diameter diameter [34]. Heyhat et al studied the convective heat transfer of Al_2O_3/water nanofluids in a circular tube with a constant wall temperature under turbulent flow conditions. They found that the heat transfer coefficients of nanofluids were higher than those of the base liquid (water) and increased with increasing nanoparticle concentration. The results indicated that in this system the heat transfer coefficient did not

change significantly with Reynolds number [35].

Zeinali Heris et al. studied heat transfer in both Al_2O_3/water and CuO/water nanofluids through a circular tube in laminar flow. An enhancement in convective heat transfer coefficient was observed for both particles over pure base water (41% and 38% at 3% volume fraction of Al_2O_3 and CuO nanoparticles, respectively) [15,16]. At particle volume concentrations below 2%, the heat transfer enhancement is comparable with Wen's work [21] with the enhancement rising even higher as particle volume concentration increases above 2%. This trend is consistent with the increase of thermal conductivity based on increased particle volume concentration, but the heat transfer enhancement is larger than the thermal conductivity enhancement. The results for flow at the lower particle volume concentrations are in the same range as Wen's results, showing little effect of the Reynolds number on the heat transfer enhancement. However, at volume concentrations above 2%, an increase in Reynolds number is seen to have a positive effect on heat transfer enhancement.

Namburu et al. studied the turbulent flow and heat transfer properties of nanofluids (CuO, Al_2O_3 and SiO_2) in an ethylene glycol and water mixture flowing through a circular tube under a constant heat flux. They concluded that nanofluids containing smaller diameter nanoparticles had higher viscosities and Nusselt numbers [11]. Putra et al. [36] have reported the suppression of the natural convective heat transfer in a nanofluid of Al_2O_3/water and CuO/water. They found out that this could be because of the settling of the nanoparticles and the velocity difference between the nanoparticles and the main fluid. Pak and Cho studied heat transfer performance of Al_2O_3/water and TiO_2/water nanofluids flowing in a horizontal circular tube with a constant heat flux under turbulent flow

conditions. The results showed that the Nusselt number of the nanofluid increased with increasing Reynolds number and volume fraction. On the other hand, the results revealed that heat transfer coefficient of the nanofluid with 3% volume fraction nanoparticles was 12% lower than that of pure water [37].

Mostafa Jalal et al. have performed an experimental study of the impact of a CuO/water nanofluid on the convective heat transfer of a heat sink in the laminar flow regime. They found that the heat transfer coefficient increased with increasing volume fraction of nanoparticles [8]. Fotukian and Nasr Esfahani studied the heat transfer coefficient of CuO/water nanofluid in a circular tube under turbulent flow conditions. They found that the heat transfer coefficient was enhanced by 25% at 0.015% and 0.236% (volume fraction). No significant variation in the heat transfer enhancement ratio based on the concentration of CuO nanoparticles was observed [38]. Li et al. [39] experimentally investigated a 35 nm Cu/deionized water nanofluid flowing in a tube with constant wall heat flux. They showed that the ratio of the Nusselt number for the nanofluid to that of pure water under the same flow velocity varies from 1.05 to 1.14 by increasing the volume fraction of nanoparticles from 0.5% to 1.2%, respectively. In other words, the heat transfer performance was enhanced by a maximum of 14% by using Cu/water nanofluids. Xuan et al. [40] reported heat transfer of Cu/water nanofluid under constant wall heat flux in turbulent flow regime and concluded that convective heat transfer enhancement of the nanofluid may be related to the thermal conductivity increase or the random movement and dispersion of nanoparticles within nanofluid. Some of the results discussed above are summarized in Table 1.2.

Table 1.2 Heat transfer enhancements

Author/Year	Nanofluid	Particle size (nm)	Concentration (vol%)	Enhancement ratio
Putra et al./2003[36]	Al_2O_3/water	131.2	1.00	0.85 – 1.02
	(L/D=0.5)	131.2	4.00	0.70 – 0.85
	Al_2O_3/water	131.2	1.00	0.87 – 1.04
	(L/D=1.0)	131.2	1.00	0.63 – 0.82
Xuan et al./2003[40]	Cu/water	<100	0.30	0.99 – 1.05
		<100	0.50	1.01 – 1.08
		<100	0.80	1.07 – 1.13
		<100	1.00	1.13 – 1.15
		<100	1.20	1.14 – 1.21
		<100	1.50	1.23 – 1.27
		<100	2.00	1.25 – 1.35
Wen et al./2004[21]	Al_2O_3/water	42	0.60	1.04 – 1.12
	(x/D=63)	42	1.00	1.09 – 1.22
		42	1.60	1.25 – 1.38
	Al_2O_3/water	42	0.60	1.10 – 1.20
	(x/D=116)	42	1.00	1.12 – 1.20
		42	1.60	1.26 – 1.35

Overall, adding nanoparticles to heat transfer fluids seems to improve the heat transfer properties of the fluid. It seems that in most cases the heat transfer coefficient

enhancement increased with increasing Re and volume fraction, however, in some cases no changes were observed and even negative enhancements have been observed by increasing volume fraction. Heat transfer coefficients generally appear to increase with decreasing nanoparticle size. Due to the inconsistencies within the research conclusions of these experimental works, a number of groups have turned to theoretical and simulation studies to better explain the possible mechanisms behind heat transfer enhancement without the variability introduced by the measurement systems.

1.5 Theory And Simulation Of Heat Transfer Of Nanofluids

To better understand how the nanoparticles influence the thermal physical properties of nanofluids, the kinematics and dynamics of the nanoparticles have been investigated in a number of simulation studies. Researche on theory and simulation of heat transfer of nanofluids are discussed below.

Akbarnia and Behzadmehr reported a CFD model for the investigation of the laminar convection of a water/Al_2O_3 nanofluid in a horizontal curved tube. Their study focused on theeffects of nanoparticle concentration. For a given Reynold number, the nanoparticle concentration was shown to have a positive effect on the heat transfer enhancement [41]. Mirmasoumi and Bezadmehr have used a two-phase model on the same system for the prediction of turbulent forced convection in a tube with uniform heat flux. In the CFD simulation the effect of nanoparticle volume fraction on the hydrodynamic and thermal parameters was investigated. Their results showed that increasing the nanoparticle volume fraction augments the molecular thermal diffusion, which significantly enhances

the heat transfer enhancement [42]. Aminfar and Motallebzadeh investigated the concentration distribution and velocity field of nanoparticles of a water/Al_2O_3 nanofluid in a pipe with a constant heat flux based on a Lagrangian-Eulerian model in the laminar regime. They reported that the Brownian force has the greatest impact on the nanoparticle concentration distribution and velocity field when compared to other forces such as thermophoretic and gravitational forces [43].

Kumar investigated the heat transfer enhancement numerically using the single-phase approach for constant wall temperature boundary condition in both the laminar and turbulent flow regime in a pipe using a Al_2O_3 nanofluid. Both the experimental values and the numerical predictions showed that the heat transfer enhancement in the laminar regime is not as significant as in the turbulent regime. It should be noted though that the single-phase approach does not predict heat transfer coefficient in laminar as accurately as in the turbulent regime. Maybe because in turbulent flow particles could be considered as the main flow but in laminar flow particles should be considered as a second phase [44]. More research needs to be done to arrive at a definitive conclusion on the efficacy of a single-phase approach for laminar flow heat transfer prediction. Jin conducted numerical simulations of the two-phase flow of Cu/water nanofluids through a pipe using Eulerian-Lagrangian approach in both the laminar and turbulent regime. The results indicated that in laminar flow with plug inlet flow, nanoparticles travel toward the centerline and lead to a non-uniform particle concentration. On the other hand with the fully developed boundary conditions at the inlet, nanoparticles travel parallel to the pipe wall, and the original concentration will be conserved. In addition, particle dispersion in fully developed turbulent flow is not uniform, more particles are present in the region of $0.65<r/R<0.95$

[45].

In this study, the enhancement of the heat transfer coefficient is determined experimentally using a CuO based nanofluids by dispersing CuO nanoparticles (40nm) with different particle loadings (0.25%, 1% and 2%wt) into water. Initial fluid temperatures are set 40, 60 and 70°C for individual experimental runs. The experimental results illustrate that various factors including Reynolds number and particle concentration are all capable of impacting the enhancement ratio though not in a consistently predictable way. To further explain the impact of these variable on the thermal parameters of a nanofluid, we developed a CFD simulation. The subsequent chapters discuss the experimental procedures and the theory used in the development of the simulation, as well as the results from both experimental and theoretical.

CHAPTER II

METHODS AND MATERIALS

2.1 Experiments

2.1.1 Preparation of CuO/water Nanofluids

Preparation of nanofluids is the first key step in applying nanoparticles to change heat transfer performance of conventional fluids. To study the effect of dispersant on stability of the solution, sodium nitaratecitarate is used as dispersant at different concentrations. Spherical shaped copper oxide nanopowders (purity: 99.9%, particle size 40nm) obtained from Skyspring Nanomaterials (Houston, Texas, USA) were suspended in pure water at weight percentages of 0.25%, 1.0% and 2.0% using ultrasonic vibration, a Model 500 Sonic Dismembrator from Fisher Scientific (shown in figure 2.1) for 30min and shaken well before further testing.

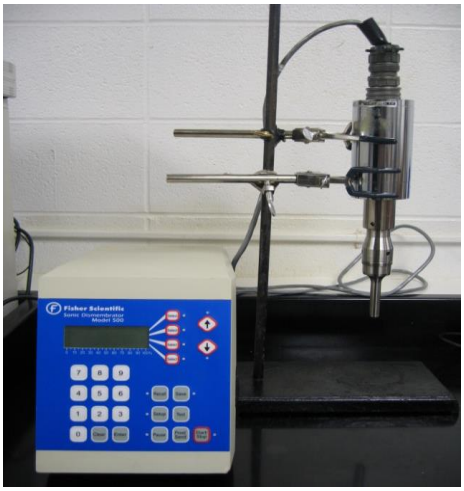

Figure 2.1 Model 500 Sonic Dismembrator.

Results revealed that samples with no dispersant had a good stability as it is shown in figure 2.2 compared to the samples with sodium nitaratecitarate as a dispersant. Based on this, it was decided that the nanofluids would be made without dispersant.

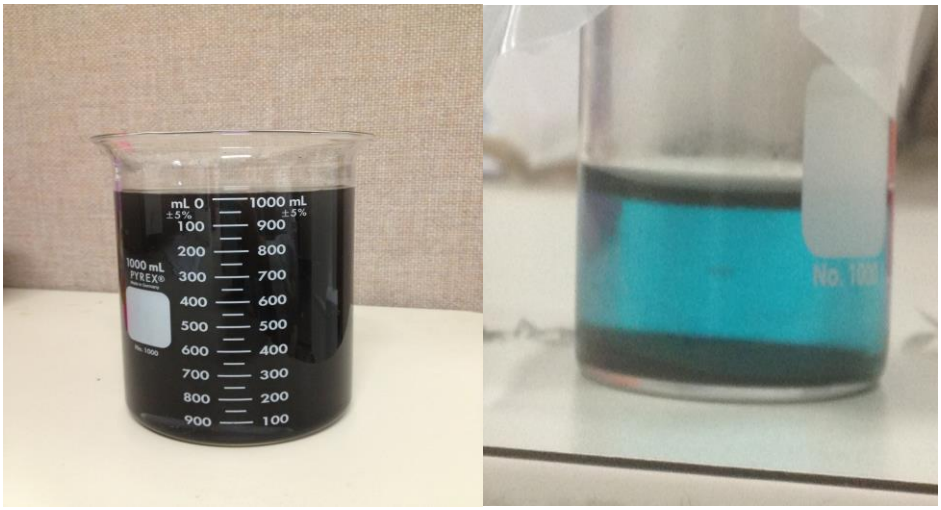

a) **b)**

Figure 2.2. CuO/water nanofluid samples a) without dispersant b) with sodium nitaratecitarate as dispersant

2.1.2 Experimental Setup

Heat transfer coefficients of prepared base and nanofluids were measured using a lab-built test rig. A schematic of heat transfer test rig is shown in Figure 2.3. The entire system is made from ¼ inch stock copper tubing and fittings. In the flow system, a copper pipe serves as a reservoir for the nanofluids and is capable of holding 2 liters of fluid. The fluid flows from the reservoir through a variable speed gear pump (Grainger 6NY97). The gear pump is sized to cover a wide range of flowrates up to 4.8 gal/min. Based on the properties of the nanofluid, particularly viscosity, the pump can cover a Re range from 50 to 7000. Flowrates are measured using an inline flowmeter connected into an electronic readout. From here the fluid flows through a copper coil held in a hot water bath which can maintain the test fluid at any temperature from room temperature up to 96°C. The fluid then enters the heat exchange section. There are two thermocouples placed in the fluid at both the inlet and outlet of this section. The section itself is formed form ¼ inch high thermal conductivity copper refrigerator tubing. Six type-T thermocouples are attached equidistant along the exterior of the copper tube in this section. The entire heat exchange section is wrapped in heat tape which provides a constant heat flux to the fluid. Two layers of insulation are wrapped around the heating tape to ensure low heat loses within the heat exchange section. Temperatures are monitored in real time using a Labview program designed for the system. The program also provides real time calculation of the heat transfer coefficient based on the fluid properties and flowrates. The heat transfer coefficient enhancement ratio at fluid temperatures of 40, 60 and 70°C and different CuO concentrations were calculated from experimental measurements.

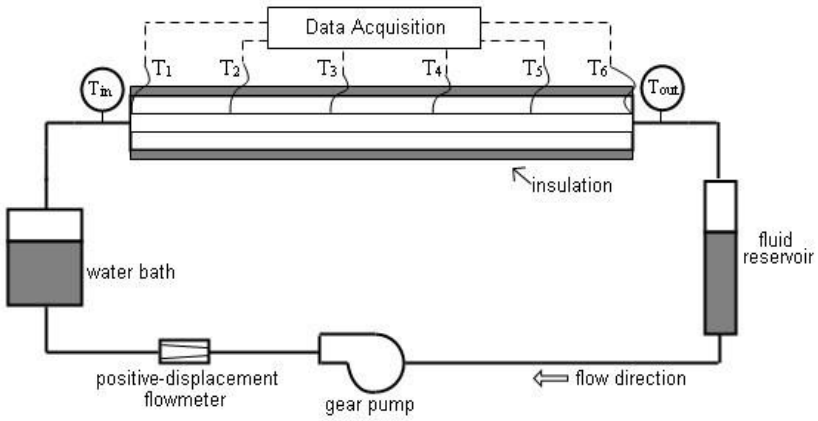

Figure 2.3. Schematic of heat transfer test rig.

The heat transfer measurement procedures are: 1) set up water bath temperature and fill the reservoir with test fluid; 2) Start the pump and circulate the fluid until inlet fluid temperature is stable at the bath temperature; 3) Set up desired flow rate and heating tape power; 4) Record data after the system reaches steady state (usually in 20-30min). By using control variables including heating power, inlet fluid temperature and fluid flow rate, a series of heat transfer coefficient tests were conducted on the base and nanofluids. The ratio of heat transfer coefficient of nanofluid to base fluid was calculated to determine if there was any enhancement.

To prevent coating of the nanoparticles inside the heat transfer test rig, kerosene was used to flush the system twice for 20mins when switching test fluids. For preliminary tests, hexane was used after the kerosene flush to flush the residual kerosene. Due to the low boiling point of hexane (69°C), we could elevate the water bath temperature to evaporate any residual hexane within the system.

2.1.3 Experimental Calculations

Heat transfer coefficient is the proportionality constant between the heat flux and the thermodynamic driving force for the flow of heat and shows how effectively heat can be transferred within a system. Heat transfer coefficient is defined by:

$$h = \frac{\mathrm{D}Q}{A \cdot \mathrm{D}T \cdot \mathrm{D}t} \tag{2.1}$$

where ΔQ is the heat input or heat loss, A is the surface area, ΔT is the temperature difference between solid surface and surrounding fluid, and Δt is the time period.

In this study, heat transfer coefficient is calculated using the following equation:

$$h = \frac{\frac{(T_{out} - T_{in}).c_p \,.\rho.Q}{\pi.d.L}}{\Delta T} \tag{2.2}$$

where T_{out} and T_{in} are the outlet and the inlet temperatures of the heat exchange section, respectively. c_p is the specific heat of the fluid, ρ is the density of the fluid, Q is volumetric flow rate, and d and L are the diameter of the tube and total length of the heat exchange section, respectively. ΔT, which represents the driving force for heat transfer, is the average temperature difference between surface of the tube and the fluid.

A common dimensionless value used in heat transfer calculations is called the Nusselt number *Nu,* named after Wilhelm Nusselt. The Nusselt number is the ratio of convective to conductive heat transfer across the boundary of heat transfer, which is defined as:

$$Nu = \frac{h.D}{k} \tag{2.3}$$

where h is the heat transfer coefficient, D is the diameter of the tube, and k is thermal

conductivity of the fluid.

The density of nanofluids is calculated using the correlation proposed by Pak and Cho [36], which is defined as:

$$\rho_{nf} = \phi \cdot \rho_p + (1-\phi)\rho_{bf} \tag{2.4}$$

where ρ_{nf} is the density of the nanofluid, ϕ is the volume fraction of the nanoparticles, and ρ_p and ρ_{bf} are the densities of the CuO nanoparticle and base fluid, respectively.

Another dimensionless value commonly used in heat transfer calculations is the Reynolds number *Re*, named after Osborne Reynolds. The Reynolds number is the ratio of momentum forces to viscous forces which is defined as:

$$\mathrm{Re} = \frac{rVL}{m} \tag{2.5}$$

where ρ is the density of the test fluid, V is the mean velocity of the test fluid, L is the diameter of the test tube, and μ is the dynamic viscosity of the fluid.

Viscosity of the CuO/water nanofluids is assumed to be the same as water viscosity because the volume fraction of CuO is very small (CuO volume fractions are 0.00155, 0.000388 and 0.0031) in these experiments.

Heat capacities of CuO/water nanofluids are calculated using a theoretical model based on the assumption of thermal equilibrium between the particles and the surrounding fluid [45, 46]:

$$C_{p,nf} = \frac{\rho_{np}\phi_{np}C_{p,np} + \rho_f\phi_f C_{p,f}}{\rho_{np}\phi_{np} + \rho_f\phi_f} \tag{2.6}$$

where C_p is specific heat, ϕ is the volume fraction, ρ is the density, and the subscripts np, nf, and f refer to nanoparticle, nanofluid, and base fluid, respectively.

2.2 Simulation Configurations

Understanding flow behavior, particle behavior near the wall, and particle migration in nanofluids is important for future utilization of nanofluids as potential heat transfer media. We performed numerical simulations of CuO/ water nanofluid two phase flows by using an Eulerian-Lagragian approach to study the nature of both the laminar and turbulent flow fields of the fluid phase as well as the kinematics and dynamics of the dispersed nanoparticles. The Eulerian-Lagrangian method is used to track the trajectory of an individual stream of nanoparticles to illustrate the particle motion relative to the wall and to each other.

For this purpose, the commercial CFD solver FLUENT was used to perform the simulations to model nanofluids travelling in a pipe. The particles selected are spherical copper oxide nanoparticles with a 40nm diameter and a density of 6.4 g/cm^3. During the simulation, the CuO nanoparticle concentrations are maintained at 0.25% and 1% by weight. The simulation systems adapted for this work are presented herein. The geometry of the computational domain, mesh configuration, materials and theoretical methods that have been employed in the simulation are also described.

2.2.1 Geometry and Mesh Configuration

To make this work more realistic, a pipe flow, which is one of the most common configurations in industry, with 0.0048 m in diameter and 1.095 m in length (shown in Figure 2.4) is considered. This matches the geometry of the heat exchange section of the measurement system used in the experimental measurements.

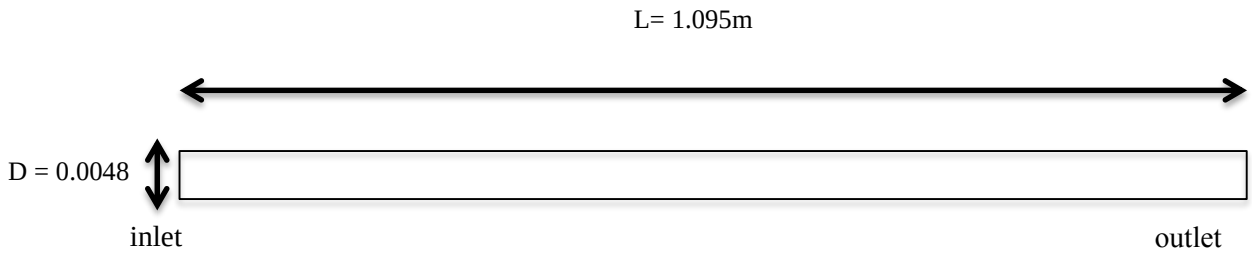

Figure 2.4. Geometry of computational cell

One of the purposes of doing this simulation is to capture and understand the near wall behavior of the nanoparticles. Therefore, a better resolution or a relatively fine mesh in the near wall area or in the boundary layer is needed. However, a low computational effort requires that the mesh should not be too fine. The mesh we used in this work is shown in Figure 2.5.

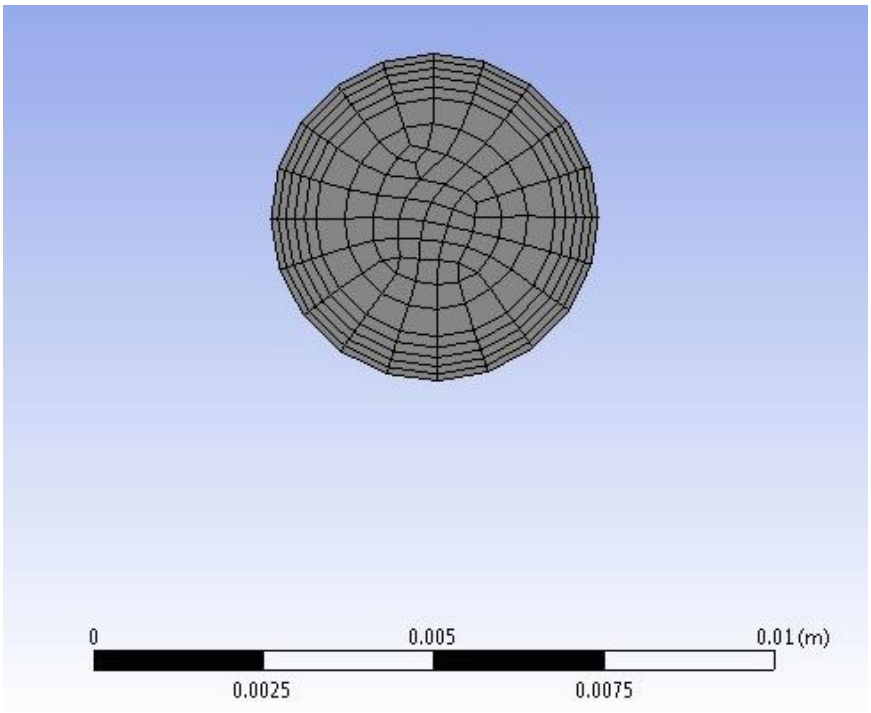

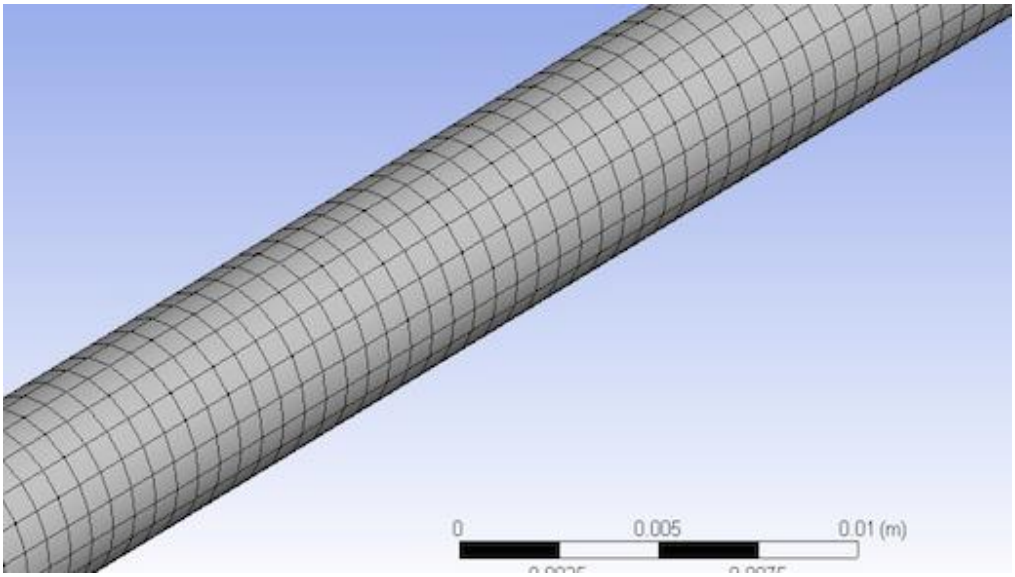

Figure 2.5. Mesh Configuration at cross section of the tube and along the tube

From the figure, one can observe that there is a very fine mesh at the near wall region and a relatively coarse mesh in the area near the centerline. The results showed good convergence with this mesh. To check the mesh sensitivity 150,000, 220,000 and 263,000 nodes were used and the results revealed no changes when 220,000 and 263,000 were used. The total number of nodes in this simulation is therefor set at 263,000 based on this check of the mesh sensitivity.

2.2.2 Base fluid, Nanoparticles and Pipe Properties

The properties of the base fluid, nanoparticles and the pipe must be well defined for use in these simulations. The base fluid used in the series of simulations is water, and its properties are listed in Table 2.1. The nanoparticles used in the simulation are spherical copper oxide nanoparticles with diameter of 40 nm, and their properties are listed in Table 2.2. The properties of pipe are listed in Table 2.3.

Table 2.1. Properties of base fluid (water) at 40, 60 and 70°C

Base fluid	**Temperature (°C)**	**Density (kg/m^3)**	**Viscosity (kg/(m·s))**	**Specific Heat (J/(g·K))**
Water	40	992	0.000653	4.1785
	60	983.2	0.00046	5.1785
	70	977.8	0.000404	6.1785

Table 2.2. Property of Nanoparticles (Copper oxide)

Nanoparticle	**Density (kg/m^3)**	**Diameter (nm)**	**Thermal Conductivity (W/m·K)**
Copper oxide	6400	40	20

Table 2.3. Property of Pipe Wall

Pipe Well Material	**Density (kg/m^3)**	**Specific Heat (J/(kg·K))**	**Thermal Conductivity (W/m·K)**
Copper	8960	387	401

2.2.3 Governing Equations and Numerical Solution Strategy

The commercial CFD solver FLUENT was used to perform the simulations,

based on a finite volume approach to solve the governing equations with a coupled solver. The second-order upwind scheme was used for discretization of the convection terms, volume fraction, energy and turbulent kinetic.

Steady state simulations were carried out by solving the mass, momentum and energy conservation equations, which are expressed as:

$$\frac{\partial \rho}{\partial t} + \nabla \cdot (\rho \vec{u}) = 0 \tag{2.7}$$

$$\frac{\partial (\rho \vec{u})}{\partial t} + \nabla \cdot (\rho \vec{u} \vec{u}) = \rho g - \Delta P + \Delta \cdot (\bar{\tau}) \tag{2.8}$$

$$\frac{\partial (\rho h)}{\partial t} + \nabla \cdot \left(ph\vec{u} \right) = \nabla \cdot \left(K \nabla T + \left(\bar{\tau} \cdot \vec{u} \right) \right) \tag{2.9}$$

where h is the specific enthalpy and $\bar{\tau}$ is the viscous stress tensor which is defined as:

$$\bar{\tau} = \mu \left(\left(\nabla \vec{u} + \nabla \vec{u}^T \right) - \frac{2}{3} \nabla \cdot \vec{u} I \right) \tag{2.10}$$

These governing equations are solved by a "coupled algorithm" under the pressure-based solver in ANSYS FLUENT. In the coupled algorithm, the momentum equations and the pressure-based continuity equation are solved in a coupled manner, meaning the software solves the governing equations simultaneously. In general, the coupled algorithm significantly improves the convergence speed over the segregated algorithm; however, the memory requirement for the coupled algorithm is more than the segregated algorithm.

Both laminar and turbulent flows with Reynolds numbers up to 6.2×10^3 are examined in this study. In the laminar case, the standard Navier Stokes equations are

solved by the finite volume method provided by Fluent. In the turbulent case, the RNG k-ε model is employed. In the present study, the Eulerian-Lagrangian method is applied. The Eulerian-Lagrangian method is used to track the trajectory of an individual stream of nanoparticles to illustrate the particle motion relative to the wall and to each other. In the Eulerian-Lagrangian approach the main fluid is treated as a continuum, based on the Eulerian description. However, the dispersed particles are tracked by using the Lagrangian description where the particles can exchange momentum, mass, and energy with the main fluid phase. To track particles, three particles were injected at each of three different positions at the entrance of the tube using a cone injection type. Figure 2.6 shows the typical cone angle and radius; In this work we use cone angle of 30 and radius of 0. Injection positions were chosen near the top and bottom of the horizontal tube as well as the center of the tube. Figure 2.7 illustrates the particle injections we used in this work. The initial conditions and properties of the particle stream are assigned to the injections as well.

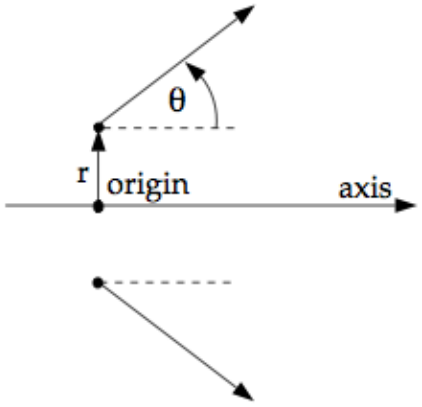

Figure 2.6. Typical cone angle and radius

Figure 2.7. Particle injection in this work

As the Lagrangian method is applied in this work, the trajectories of the particles could be displayed using the Particle Track dialog box. The particle trajectories within nanofluid with different concentrations and temperatures will be discussed in the next chapter.

During the modeling, the interaction between the fluid phase (water) and the solid phase (carbon particles) is considered and incorporated into the simulation by using two-way coupling, which means the fluid can affect the particle motion by drag, while the particles can exchange momentum and mass with the continuous fluid. The dispersion of particles due to turbulence in the fluid phase was also taken into account by using the stochastic tracking model.

The non-slip condition is used on the tube wall and for the wall thermal condition; the uniform heat flux 5897.25 (w/m^2) was applied to the entire tube as a representation of the heat tape in the experimental system. The boundary conditions for the continuum are:

- Inlet: Mass flow with velocity of 0.99 m/s parallel to axis
- Wall: Stationary wall without slip
- Axis: Axisymmetric

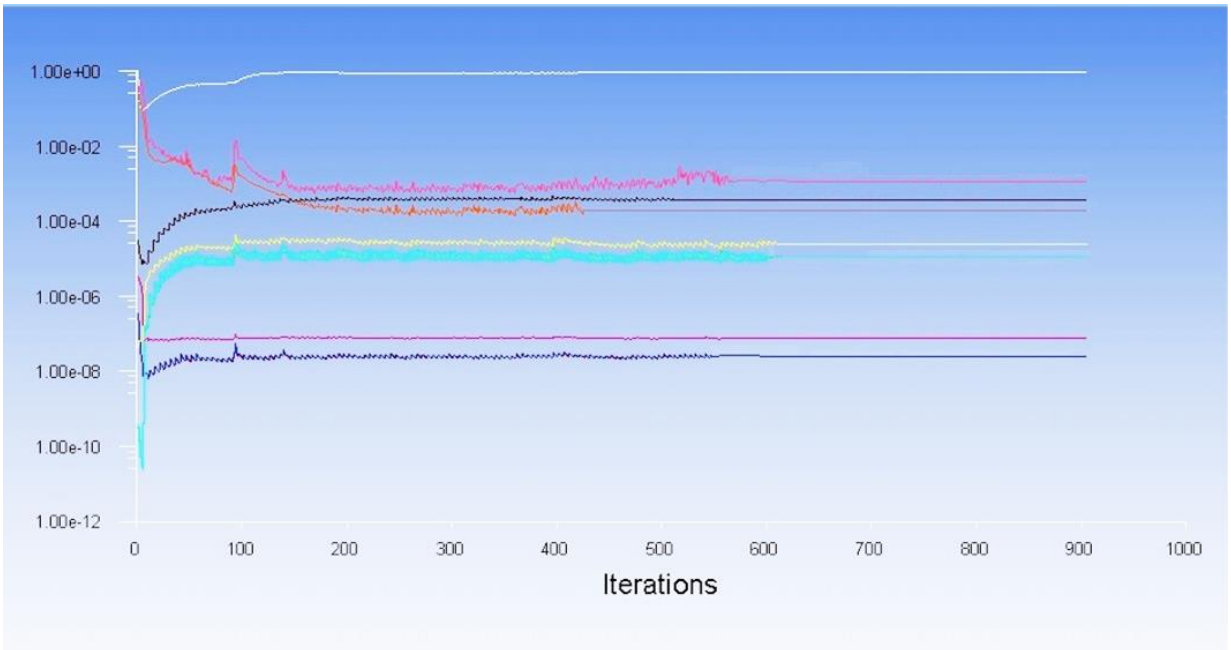

Figure 2.8 Residual convergence for turbulent flow at 70C and 0.25%wt CuO

Simulations performed where particle-particle interactions were taken into account showed no difference in fluid temperature and particle trajectory to those performed without particle-particle interactions, which suggests that particle-particle interactions are not important within this system. While this is not surprising given the low particle concentrations being used in this work, it also suggests that the impact of Brownian motion within the system is limited. This point will be discussed further in the next chapter.

To validate the model, the residual convergence as well as the convergence of the area weighted average temperature at the outlet of the tube was verified. The convergence history of flow rate, uniformity index, CuO volume fraction and turbulent dissipation rate were also checked. Figures 2.8 through 2.13 Show all these parameters for turbulent flow at 70C and 0.25%wt CuO and ensure that the solution has converged for all these parameters for 900 iterations performed in these simulations.

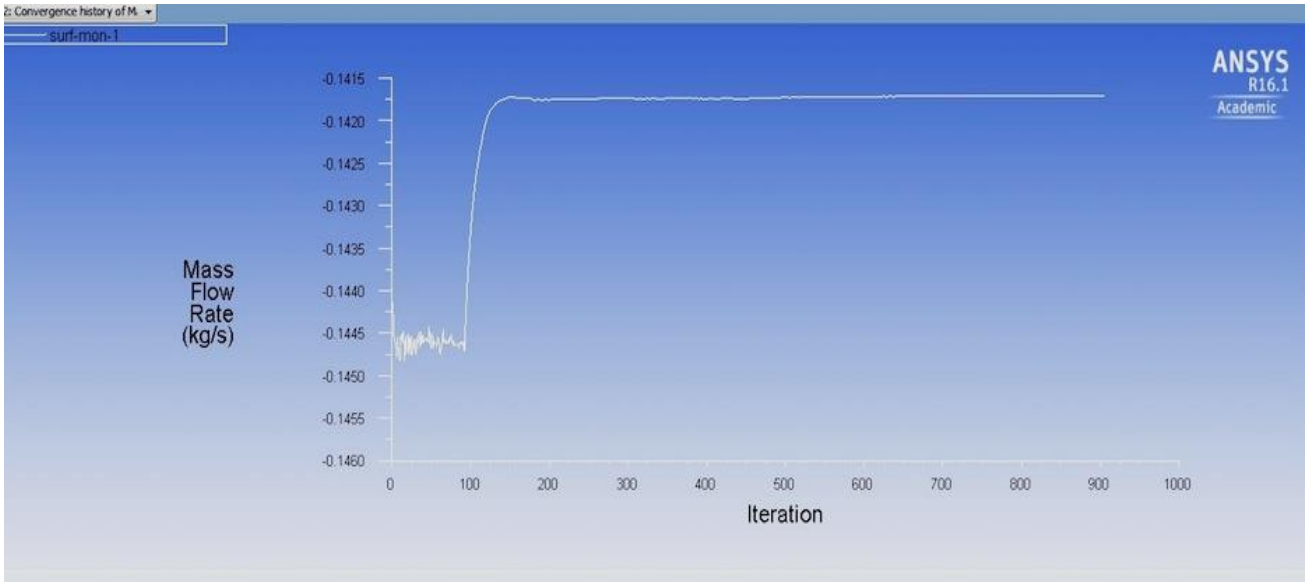

Figure 2.9 Mass flow rate convergence for turbulent flow at 70C and 0.25%wt CuO

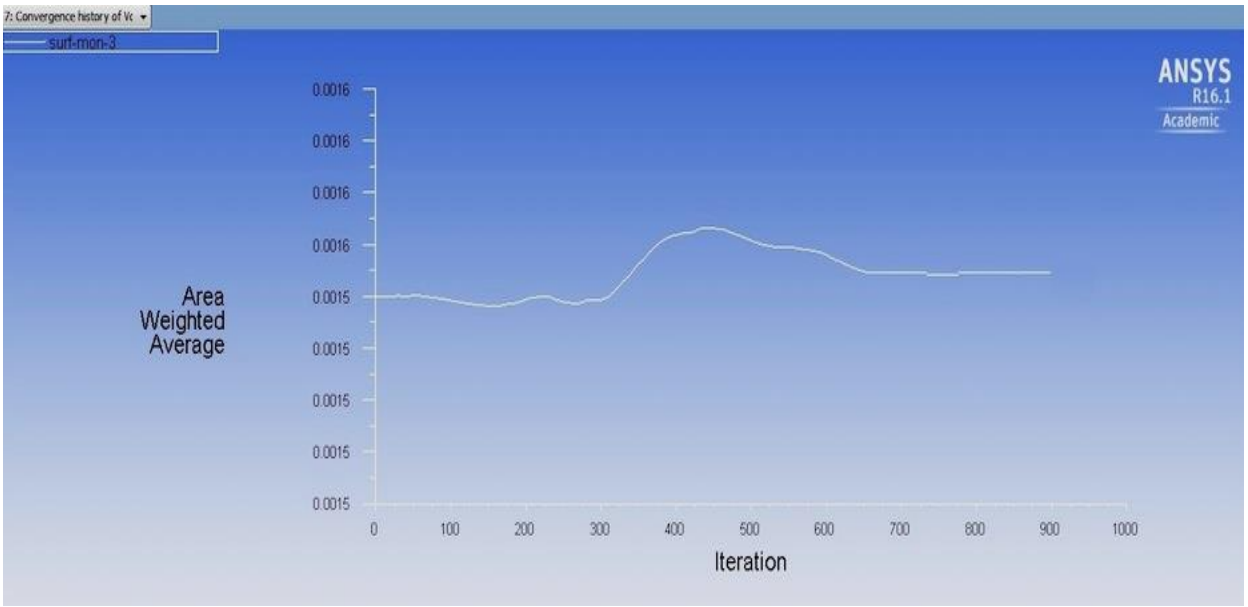

Figure 2.10 Volume fraction convergence for turbulent flow at 70C and 0.25%wt CuO

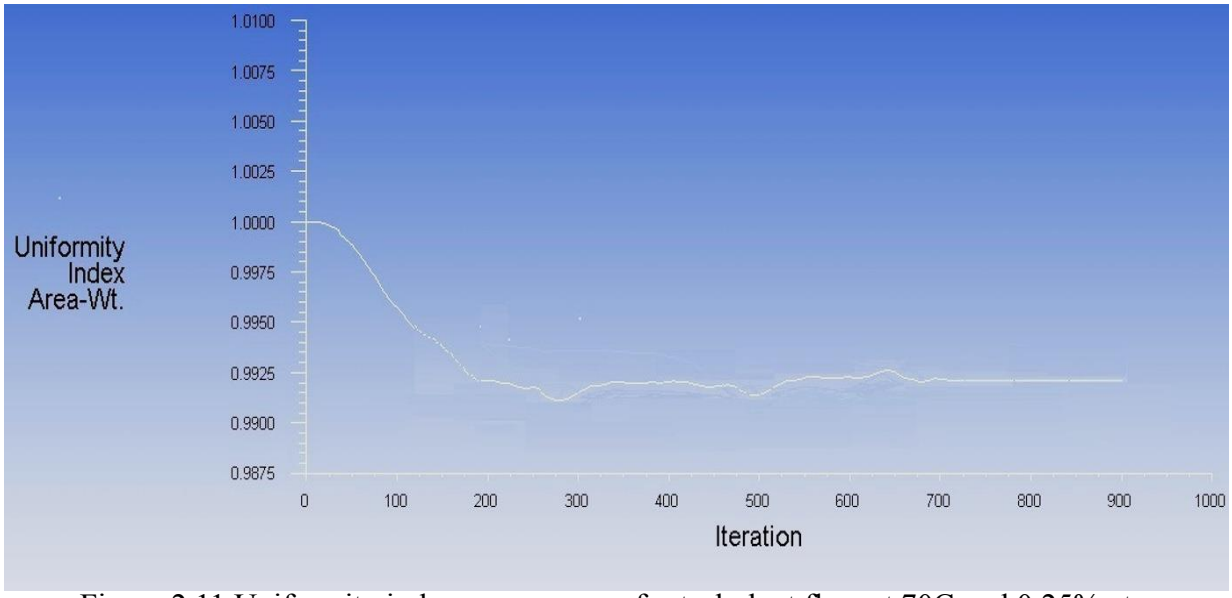

Figure 2.11 Uniformity index convergence for turbulent flow at 70C and 0.25%wt CuO

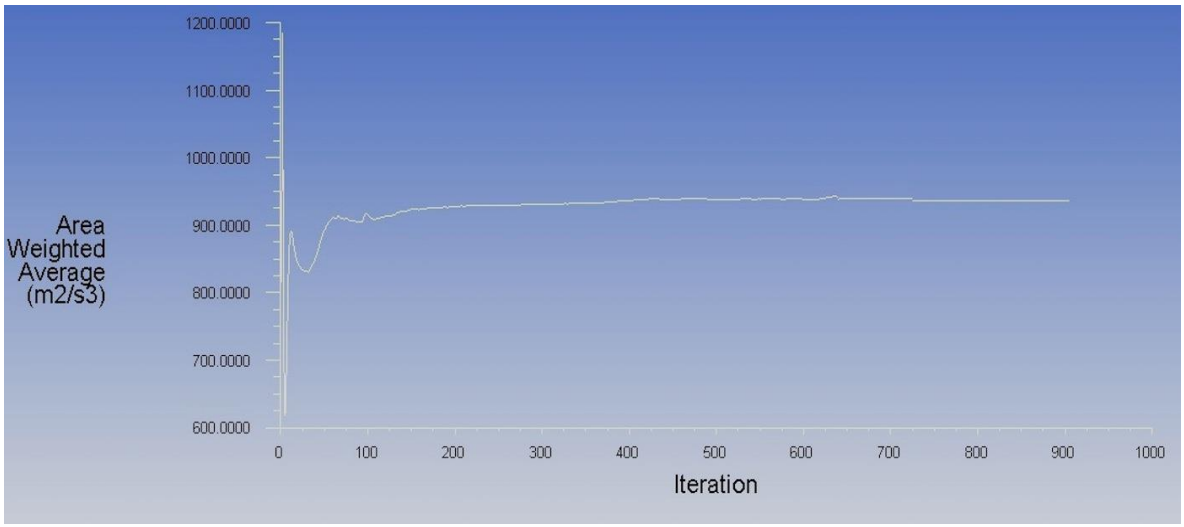

Figure 2.12 Turbulent dissipation rate convergence for turbulent flow at 70C and0.25%wt CuO

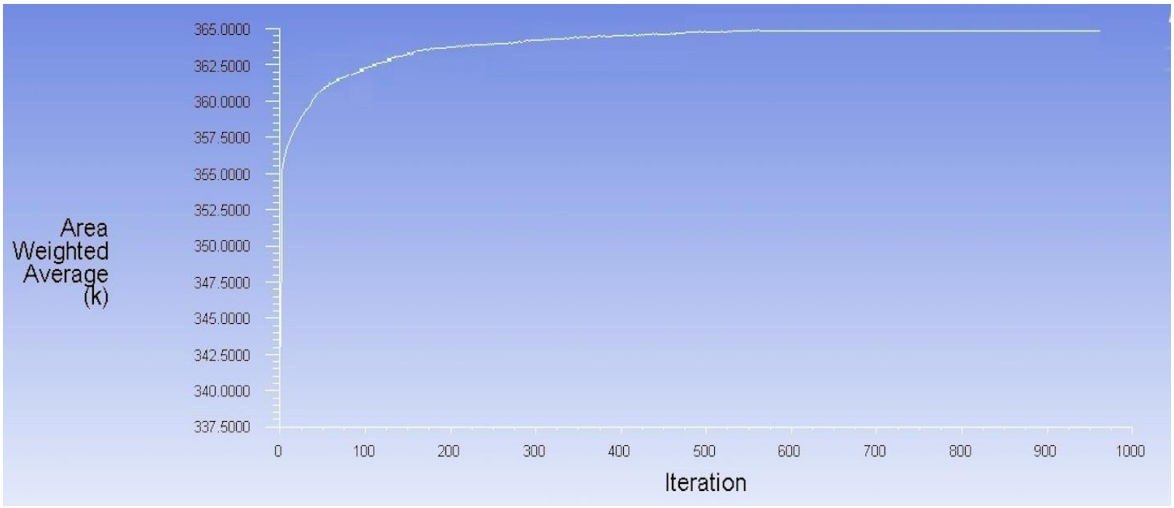

Figure 2.13 Area weighted average temperature convergence for turbulent flow at 70C and 0.25%wt CuO at outlet of the tube

CHAPTER III

RESULTS

In this chapter both experimental and simulation results are discussed. In the experimental section the heat transfer coefficient as well as the heat transfer enhancement of CuO/water nanofluids with different CuO concentrations at temperatures of 40, 60 and 70°C are shown at different flow rates. In the simulation section we focus on the 40 and 70°C results and theoretical results of both laminar and turbulent flow at each temperature are presented.

3.1 Experimental Results

Experiments using CuO/water nanofluids were conducted over a wide range of Reynolds number ($900 < Re < 6700$) covering the laminar, transition and turbulent flow regimes. The initial fluid temperature was controlled by the water bath in the heat transfer measurement system. Three temperatures (40°C, 60°C, and 70°C) were used during the measurement of the heat transfer coefficient. Figures 3.1 through 3.4 illustrate the variation in heat transfer coefficient of both water as the base fluid and several nanofluids at different nanoparticle concentrations of 0.25, 1 and 2% by weight as well as different Re numbers at temperatures of 40, 60 and 70°C. All measurements for base and nanofluids show an increasing heat transfer coefficient as the flow rate Q and Reynolds number Re increase as is expected in most cases of convective heat

transfer.

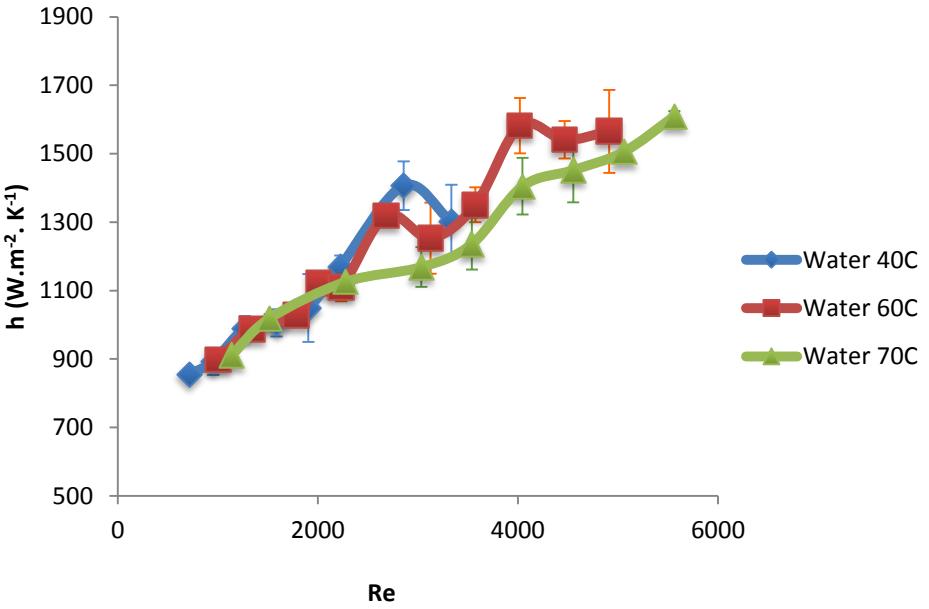

Figure 3.1. Heat transfer coefficient of water at 40, 60 and 70° C versus Re

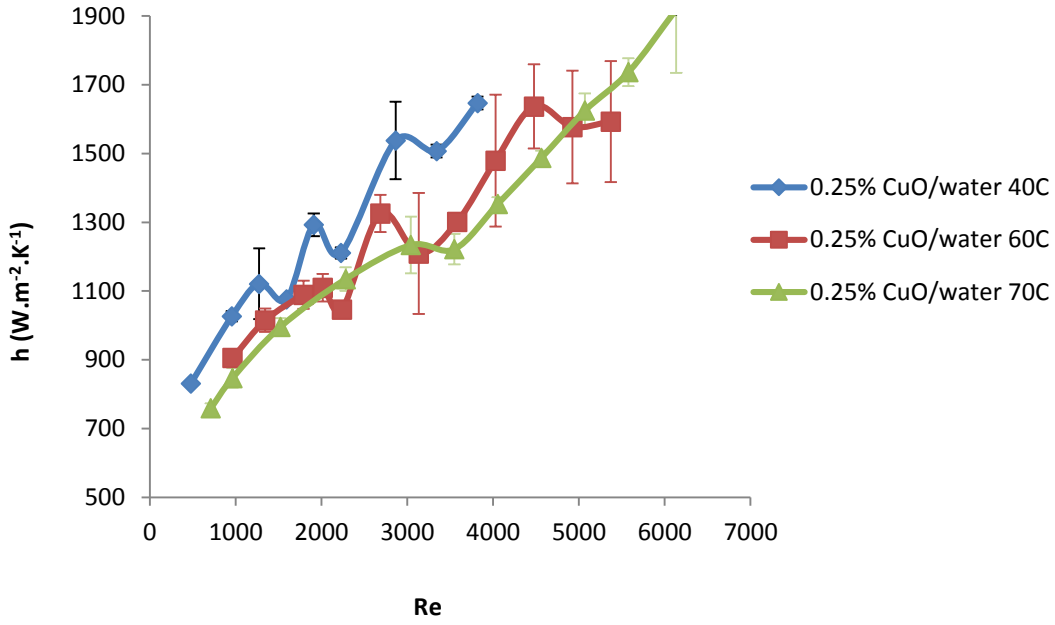

Figure 3.2. Heat transfer coefficient of CuO/water (0.25%wt) at 40, 60 and 70° C versus Re

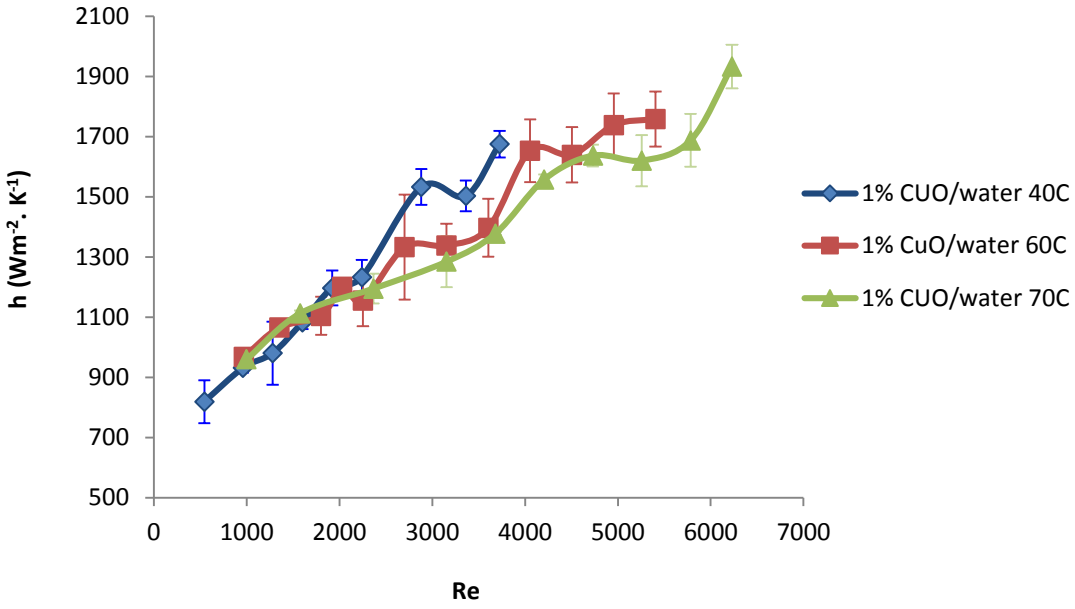

Figure 3.3. Heat transfer coefficient of CuO/water (1%wt) at 40, 60 and 70° C versus Re

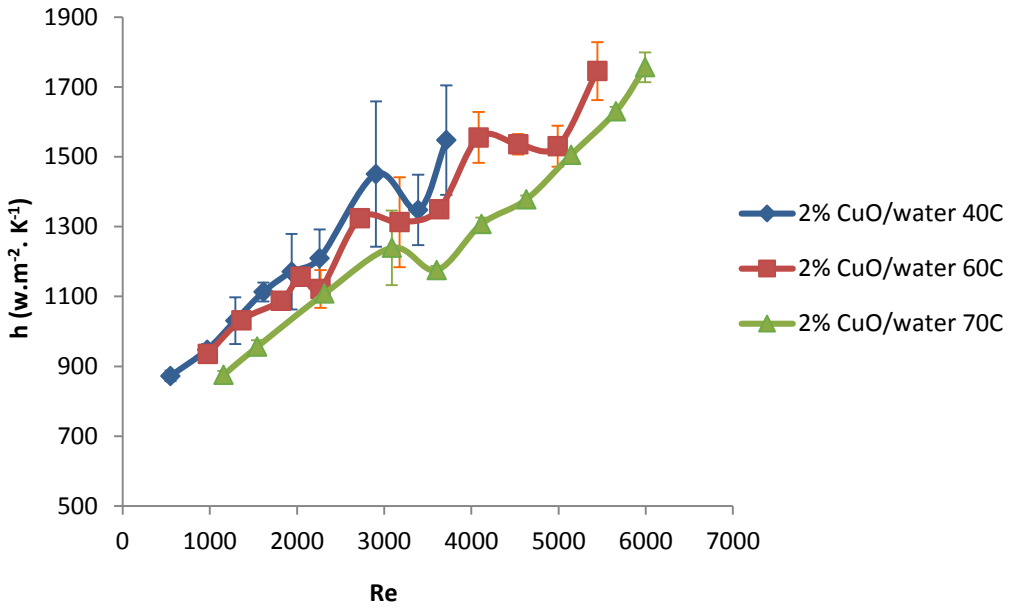

Figure 3.4. Heat transfer coefficient of CuO/water (2%wt) at 40, 60 and 70° C versus Re

The results show that at all concentrations the heat transfer coefficient is higher at lower temperatures; the same is true for pure water, though the variation is not as

pronounced as it is for the nanofluids. At the lowest temperature of 40°C, the viscosity of the nanofluid is higher which means there is less Brownian motion and collisions of the nanoparticles. The lateral movement of nanoparticles (perpendicular to the direction of the flow) is less intense compared to that at the higher temperature of 70°C where the Brownian motion is more intense. Based on the results shown in Figures 3.2-3.4 Brownian motion seems to have a negative effect on the enhancement of heat transfer coefficient, indicating that the main contribution to the enhancement of the heat transfer coefficient is the contact between the nanoparticles and the base fluid rather than the collision between the nanoparticles. Experimental data for water is almost the same within experimental error.

To demonstrate how effectively CuO nanoparticles improve the heat transfer coefficient of the base fluid, the heat transfer enhancement was determined at both 40 and 70°C. Heat transfer enhancement is defined as the ratio of heat transfer coefficient of nanofluid to the heat transfer coefficient of water. Heat transfer enhancement is more important than heat transfer coefficient in a practical way as it defines how adding nanoparticles improves the heat transfer coefficient of the nanofluids over that of water.

To calculate heat transfer enhancement the best fit linear profile was plotted for each of the nanofluids and water. At specific values of Re; the heat transfer coefficient of a specific nanofluid is divided by the heat transfer coefficient of water. Figure 3.5, 3.6, and 3.7 illustrates the heat transfer enhancement of CuO/water nanofluids at different CuO concentrations versus Re at temperatures of 40, 60 and 70°C.

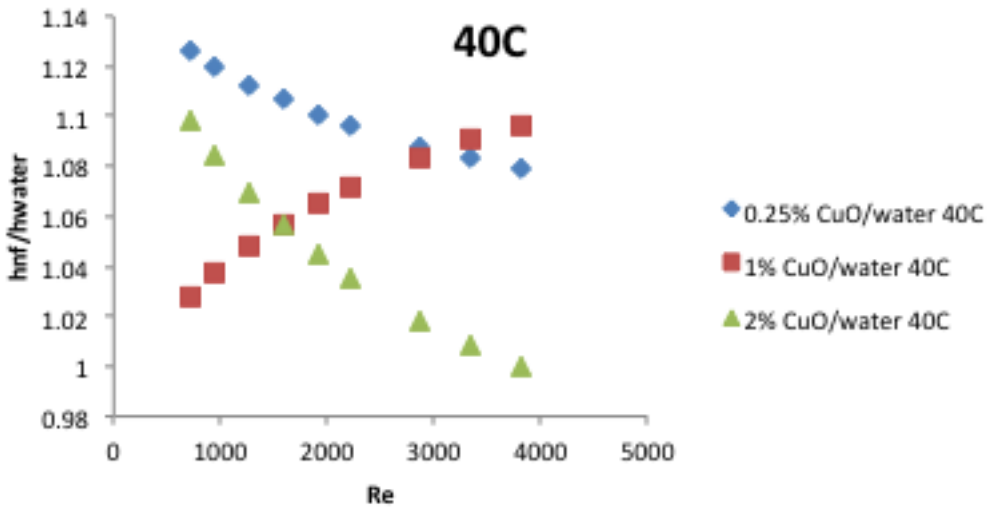

Figure 3.5. Heat transfer enhancement at CuO concentration of 0.25%, 1% and 2%wt versus Re at 40°C

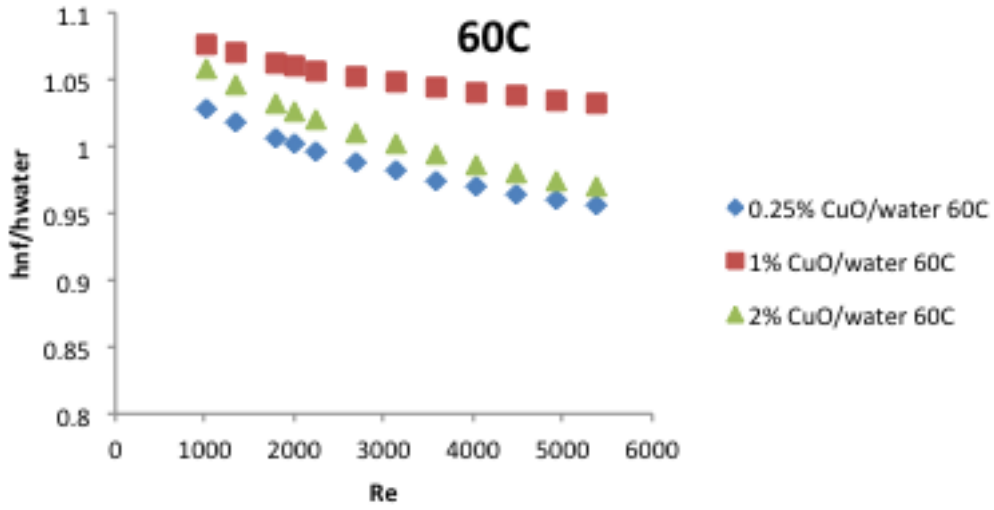

Figure 3.6. Heat transfer enhancement at CuO concentration of 0.25%, 1% and 2%wt versus Re at 60°C

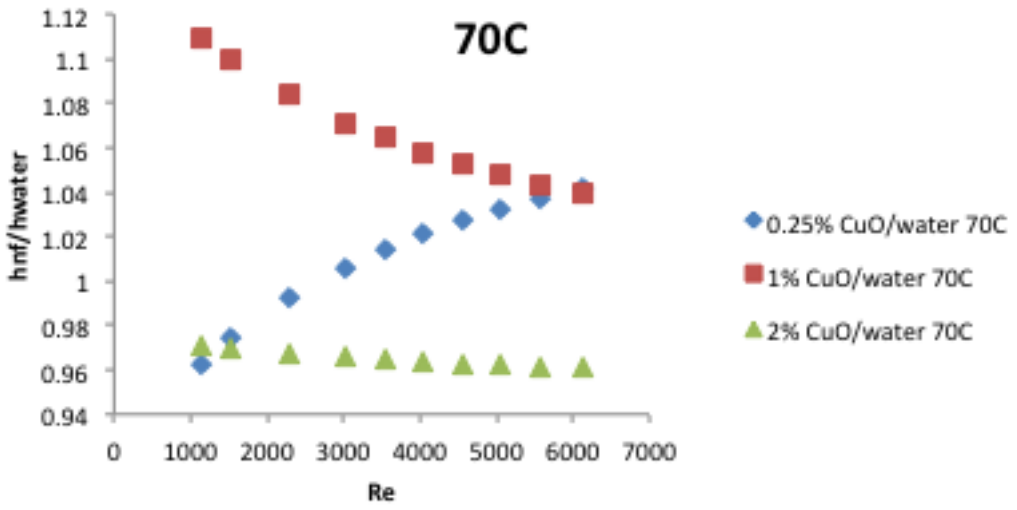

Figure 3.7. Heat transfer enhancement at CuO concentration of 0.25%, 1% and 2%wt versus Re at 70°C

The experimental results at 60°C in Figure 3.6 show that heat transfer coefficient enhancement increases initially with concentration from 0.25% to 1%wt. But, as concentration is increased further, from 1% to 2%wt, there is a decrease in the enhancement. Additionally, at all concentrations, a decreasing trend of heat transfer coefficient enhancement with respect to Re is observed. This result indicates that it is more beneficial to use nanofluids under laminar flow conditions as the enhancement is higher which is similar to the conclusions presented in other works on heat transfer in nanofluids. However, this same trend with respect to Re is not observed at all nanoparticle concentrations for the other temperatures investigated in this work.

As shown in Figure 3.5, At 40 °C the heat transfer enhancement of CuO/water with 0.25% concentration starts with a positive value at lower Re number and decreases with increasing Re. On the other hand, at the 1% concentration, the heat transfer enhancement increases with increasing Re. However, both (0.25 and 1% wt) come to almost same value of enhancement at a Re around 3000.

The opposite trend was observed at 70°C in contrast with 40°C. As Figure 3.7 shows, the heat transfer coefficient at a CuO concentration of 0.25% starts with a negative enhancement while at 1% wt the enhancement starts with a positive value. Figure 3.6 also shows that heat transfer enhancement increased with increasing Re at CuO concentration of 0.25%wt while the opposite trend was observed when a higher concentration of nanoparticles (1%wt) was used. The enhancement of 0.25 and 1% wt come to the same value at Re around 6000. It should be noted that at both temperatures, a decreasing trend in heat transfer coefficient enhancement was observed at the 2%wt nanoparticle concentration.

From Figure 3.7 one can conclude that at 70°C under laminar flow conditions, the 0.25% CuO concentration does not have practical application as it has negative enhancement, while a 11% enhancement was observed at 1% CuO concentration under the same conditions. On the other hand, at 40°C performance is better as enhancement at 0.25% is 13%, which is a relatively large enhancement given the small concentration of nanoparticles. Heat transfer coefficient enhancement at 40 and 70°C is summarized in figure 3.8 and 3.9.

Unfortunately, the observed increasing and decreasing trends cannot be explained by the experimental data alone. To understand these results, simulation needs to be done to determine these experimental behaviors with respect to the motion of the fluid and the nanoparticles.

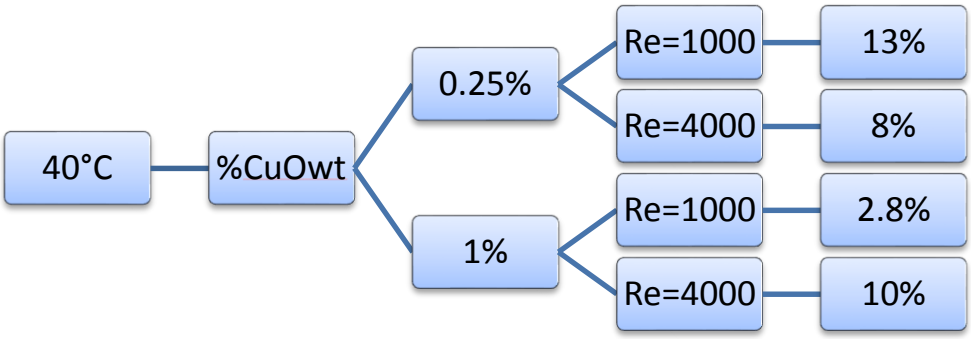

Figure 3.8 Heat transfer enhancement at 40°C

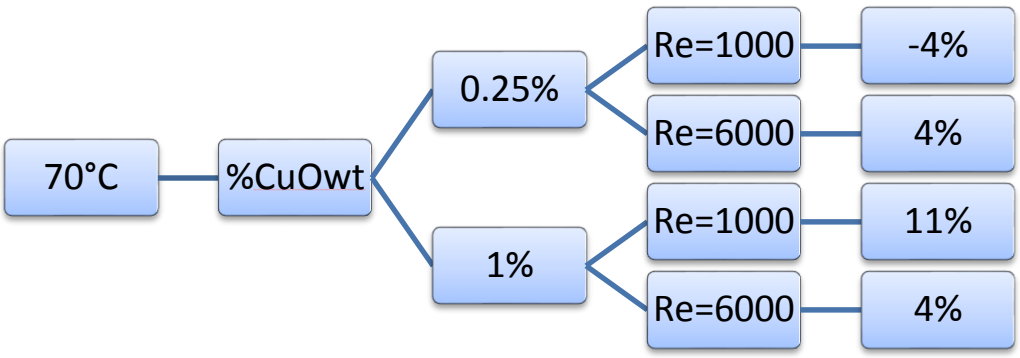

Figure 3.9 Heat transfer enhancement at 70°C

3.2 Simulation Results

To explain the observed behavior in the experimental trends of the heat transfer

enhancement of CuO/water nanofluids at different concentrations we utilized a CFD (Computational Fluid Dynamics) model for the investigation of laminar and turbulent convection of a CuO/water nanofluid at 40 and 70°C in a horizontal tube with a uniform heat flux. More details about the simulation model used in this work were discussed in Chapter 2. In this section, we discuss the simulation results in two parts. The results for 70°C are discussed first to lay the framework for understanding the experimental data. Using this framework, the simulation results are used to explain the experimental data at 40°C.

3.2.1 Simulation Results at 70°C

In order to find out how well our model matches the experimental results, the area weighted average temperature of the nanofluid should be explored. Therefore, temperature profile at three different positions along the tube was explored from the simulation and it is compared with the experimental results to see how accurate the presented model can predict the experimental results. Figures 3.10 show the model results of the temperature profile along the tube for laminar flow at 70°C of nanofluids with 0.25%wt and 1%wt CuO concentration at three positions along the tube (inlet, middle and outlet of the tube).

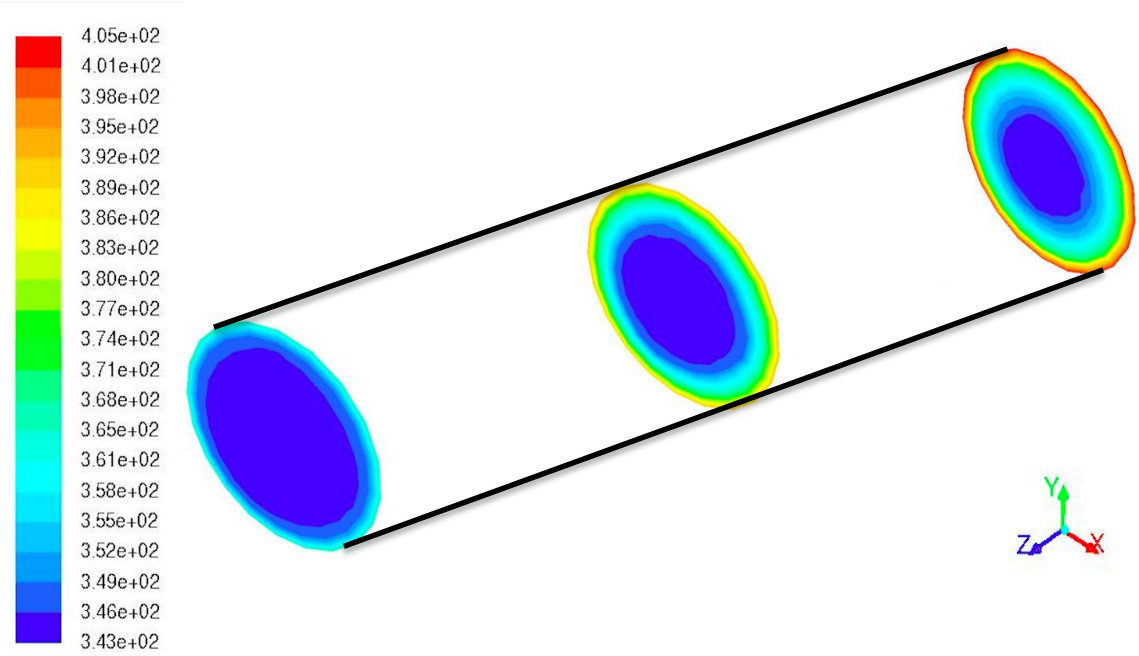

Figure 3.10. Area weighted average temperature of the nanofluid at 3 sections of the tube (Z=0, 0.5 and 1) at 70°C and 0.25%wt CuO

Table 3.1. Theoretical and experimental measurements of temperature at different locations of the tube at 0.25% CuO concentration at 70°C

Location	**Inlet**	**Middle**	**Outlet**
Theoretical Temperature (°C)	73	80.1	88
Experimental Temperature (°C)	72.16	81.1	86.8

Table 3.2. Theoretical and experimental results of temperature at different location of the tube at 1% CuO concentration at 70°C

Location	Inlet	Middle	Outlet
Theoretical Temperature (°C)	73.37	77.1	88.3
Experimental Temperature (°C)	71.9	79.2	85.9

As is illustrated in Table 3.1 the area weighted average temperatures at the inlet, middle and outlet of the tube corresponds well with experimental data from the thermocouples at these exact positions of the tube at 0.25% CuO concentration. The same conclusion can be made from Table 3.2 for 1% CuO concentration. These results confirm that our model is adequately describing the experimental data. To explain the observed experimental results of heat transfer enhancement at 70°C (Figure 3.7) we discuss the simulation results of particle migration along the tube under laminar and turbulent flow regime.

3.2.1.1 Results of Laminar Flow

As is shown in Figures 3.11 and 3.12 there is almost no motion in the radial direction for the 0.25% concentration while there is a small amount of motion of the particles near the wall in the radial direction for 1% concentration under laminar flow conditions. To understand the significance of this difference in motion of the

nanoparticles away from the wall, one must look at the location of the boundary layer under these conditions.

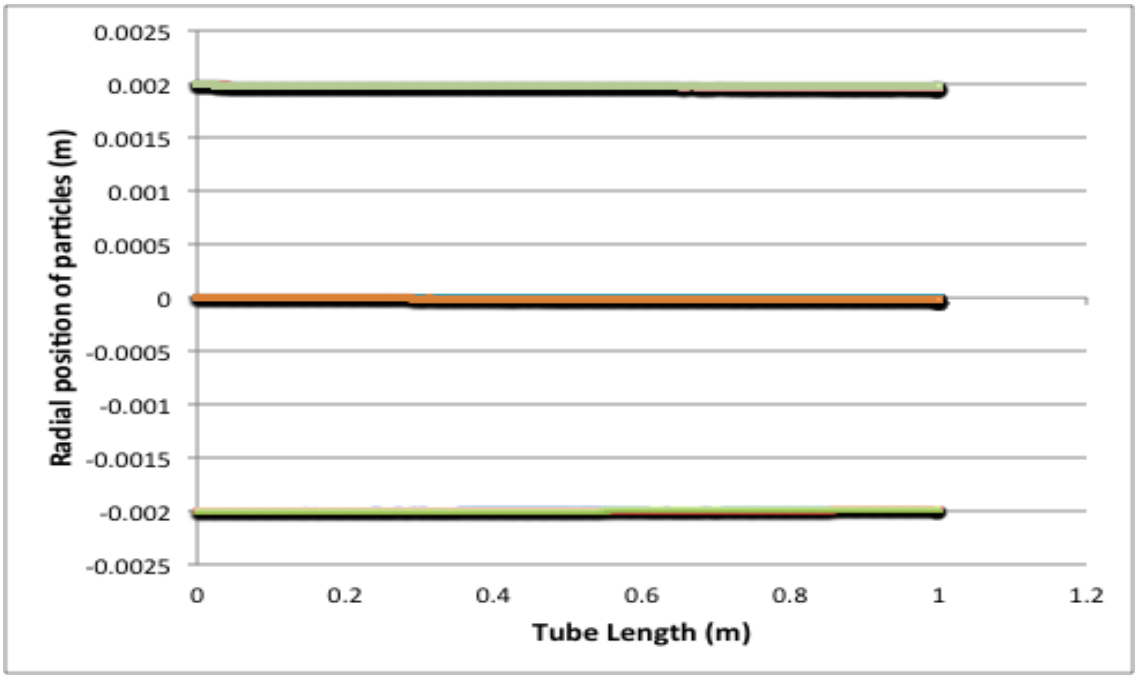

Figure 3.11. Radial position of nanoparticles of CuO/water with 0.25% concentration in laminar flow (Re=1000) at 70 at °C

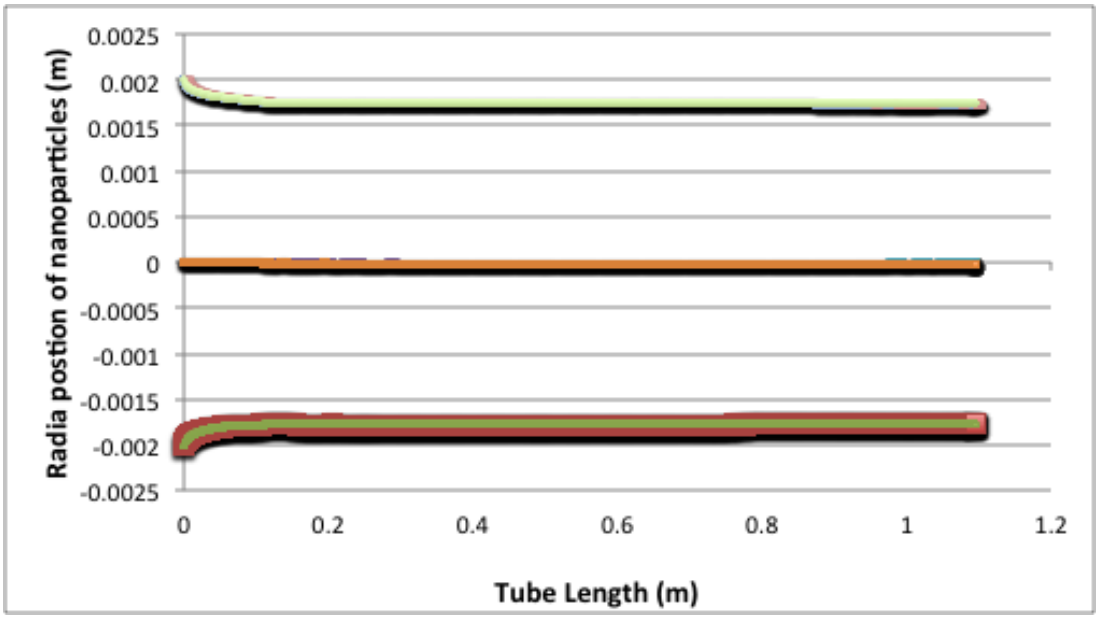

Figure 3.12. Radial position of nanoparticles of CuO/water with 1% concentration in laminar flow (Re=1000) at 70°C

The momentum boundary layer thickness, δ, is the distance from the wall to a point where the flow velocity has essentially reached the 'free stream' velocity, U_c. This distance is defined normal to the wall, at the point where the flow velocity is 99% that of the free stream stream velocity. This concept is represented in Figure 3.13.

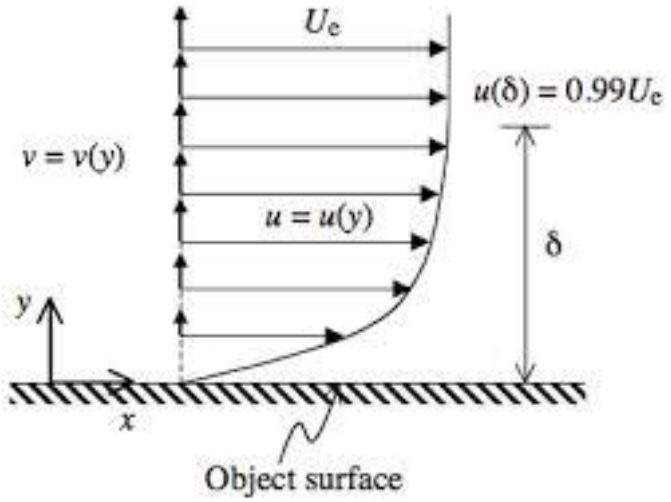

Figure 3.13. Momentum Boundary layer

The momentum boundary layer thickness has a significant effect on mass and heat transport phenomena as it is shown where the flow reaches the stream velocity. In this case if the particles can pass the momentum boundary layer they can reach the stream velocity so they can transfer heat to the bulk flow of the fluid.

The momentum boundary layer thickness and the radial position of particles within the nanofluids with 0.25 and 1% concentration along the length of the tube in laminar flow are shown in Figure 3.14. Figure 3.14 shows that particles can pass across the momentum boundary layer into the bulk flow of the fluid at the higher CuO concentration (1% CuO concentration). This gives the heated particles a better chance to transfer heat collected from near the tube wall to the bulk of the fluid because of the temperature gradient between heated particles and cooler fluid away from the tube wall.

Particles motion provides additional mixing and it will effectively enhance the heat transfer within the fluid.

At 0.25% CuO concentration though, the nanoparticles do not move through the momentum boundary layer and remain located near the tube wall so they cannot transfer heat to the bulk of the fluid. Additionally, the particles remain located near the wall such that they may partially block the fluid from contacting the wall which would lead to a decrease in convective heat transfer. Therefore, we can make the conclusion that adding nanoparticles in this case is not beneficial to the transfer of heat within the system. This evidence gives a possible explanation for why there is a higher heat transfer enhancement at higher nanoparticle concentration (1% CuO) compared to the lower concentration (0.25% CuO) in the laminar flow regime, as is observed from the experimental results which is shown in Figure 3.6.

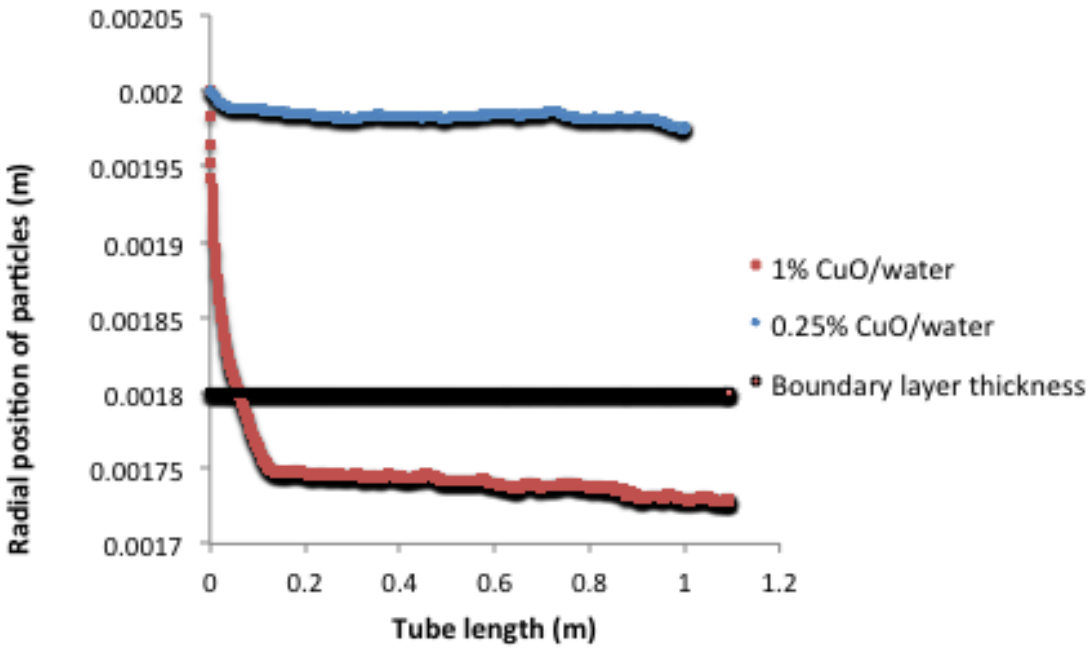

Figure 3.14. Momentum boundary layer and the radial position of particles in nanofluids with 0.25 and 1% concentration in laminar flow Re=1000 (the center of the tube is located on the vertical axis at 0)

3.2.1.2 Results of Turbulent Flow

Particle migration along the tube in turbulent flow at 0.25 and 1% concentration is illustrated in Figures 3.15 and 3.16. In both cases, the particles can cross the entire diameter of the tube and in both cases they are well mixed. This is most likely the reason the heat transfer enhancement is almost the same for both cases, as is seen in Figure 3.6.

Figure 3.15 shows that at 0.25%wt particles have much more even distribution throughout the system and they go from the wall to the fluid constantly which enables the particles to pick up heat from the wall and drop it into the bulk fluid constantly. However, the 1% case shows much more accumulation of particles near the wall and they do not have nearly as much back and forth motion. This gives rise to both concentrations giving similar enhancement values, but show why the 0.25% has an increasing trend with respect to Re, while the 1% has a decreasing trend with Re. So an increasing trend of heat transfer enhancement observed for 0.25% could be addressed by this fact that at laminar flow particle could not move through the boundary layer while in turbulent flow they can easily transfer heat from the wall to bulk fluid. On the other hand, for the 1% case particles could move through the boundary layer and they could easily transfer heat from the wall to the bulk fluid in laminar flow, while in turbulent flow particles accumulate near the wall and they do not move back and forth so adding CuO nanoparticles in this case (turbulent, 1%wt) does not improve the heat transfer coefficient of water as much as in laminar flow. Therefore, we observe a decreasing trend with Re for 1% concentration.

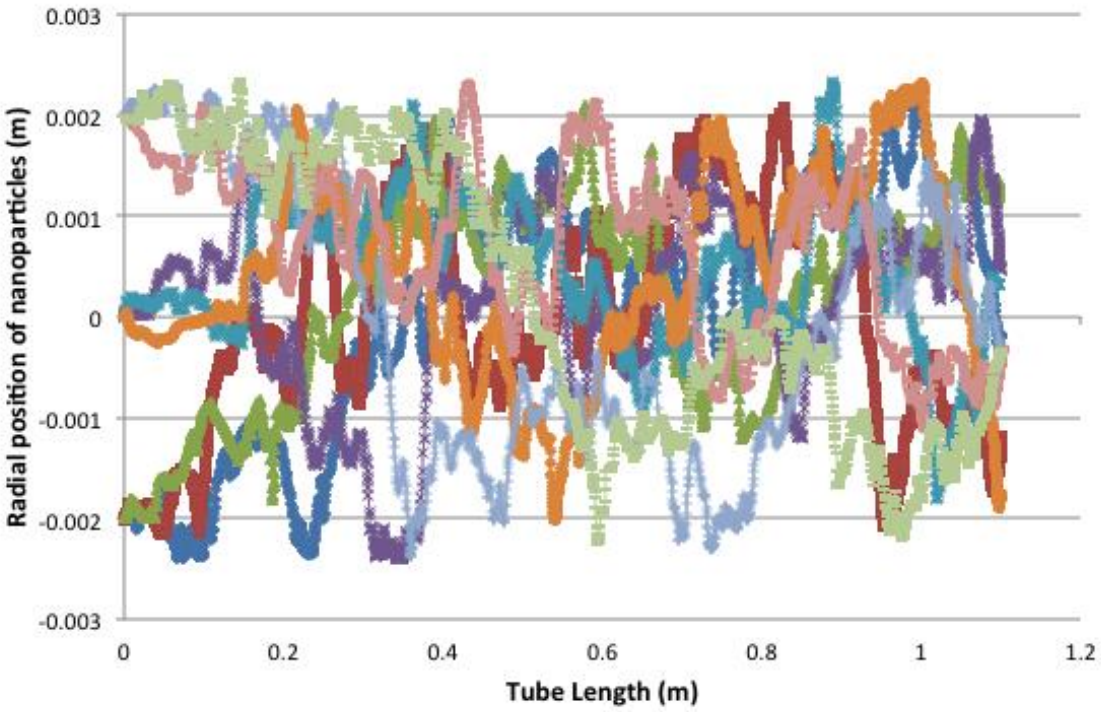

Figure 3.15. Radial position of nanoparticles of CuO/water with 0.25% concentration in turbulent flow (Re=6000) at 70°C

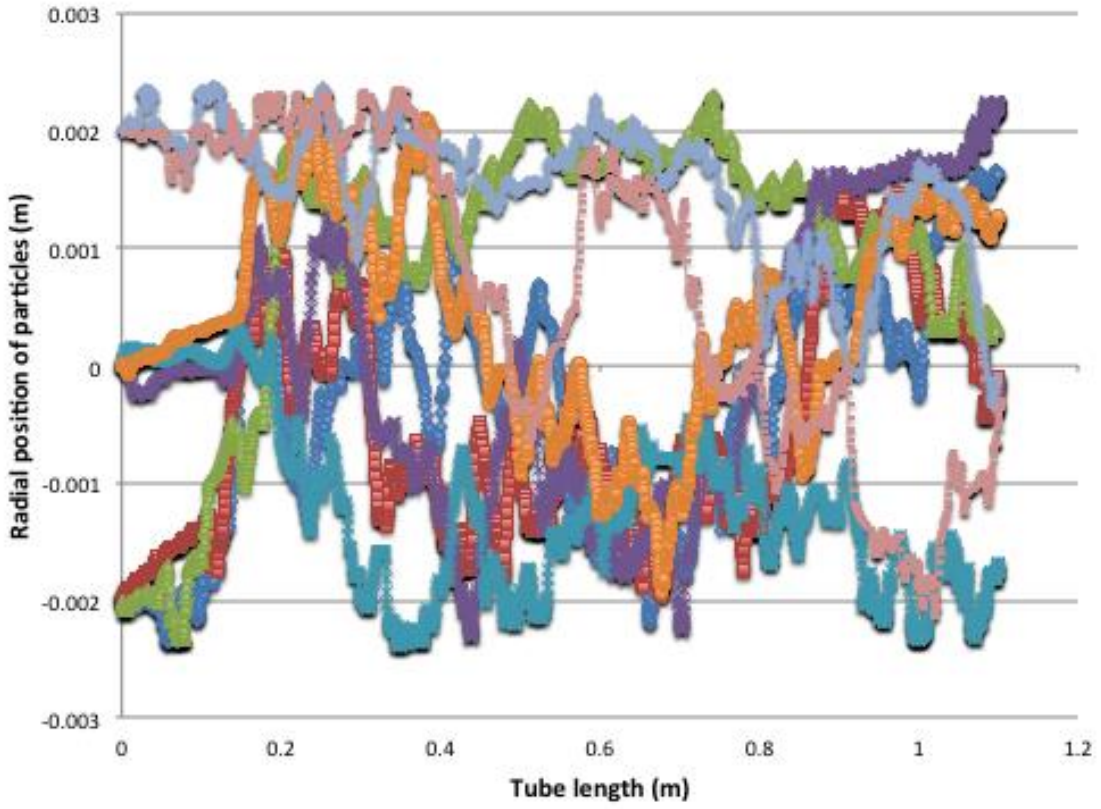

Figure 3.16. Radial position of nanoparticles of CuO/water with 1% concentration in turbulent flow (Re=6000) at 70°C

3.2.2 Simulation Results at 40°C

To check the accuracy of our model at 40 °C weighted average temperature of nanofluid is once explored. Figure 3.17 and 3.18 illustrate the temperature profile along the tube for laminar flow at 40°C at three locations along the tube (inlet, middle and outlet of the tube) at 0.25 and 1% CuO concentration respectively. As is shown in table 3.3 the area weighted average temperatures at 0.25% at the inlet, middle and outlet of the tube corresponds well with experimental data from the thermocouples at these exact positions of the tube. Area weighted average temperatures at 1% also corresponds well with experimental data (Table 3.4). These results confirm that our model at 40°C is adequately matched with the experimental data.

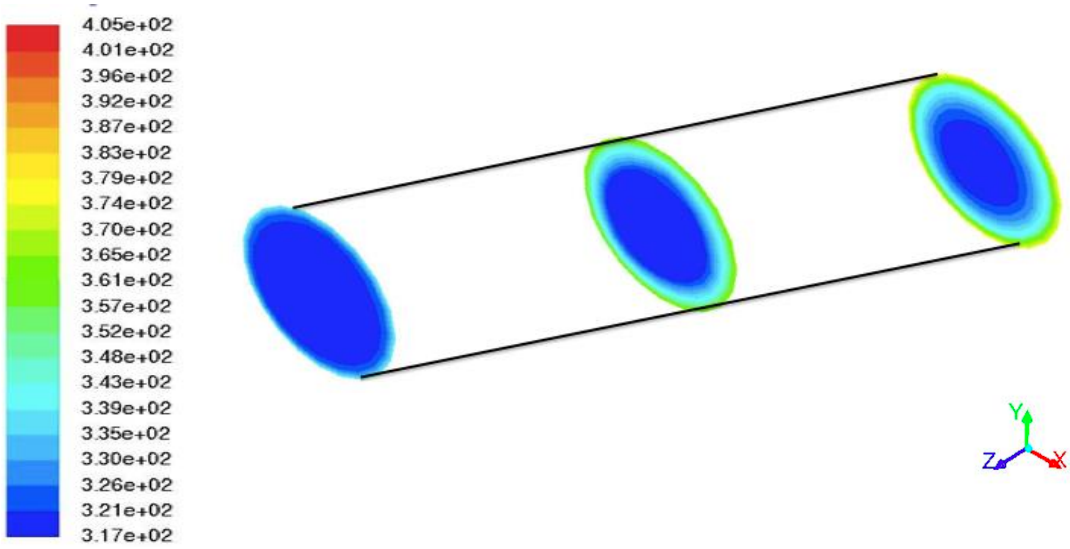

Figure 3.17 Area weighted average temperature of nanofluid at 3 sections of the tube (Z=0, 0.5 and 1) at 40°C and 0.25% CuO concentration

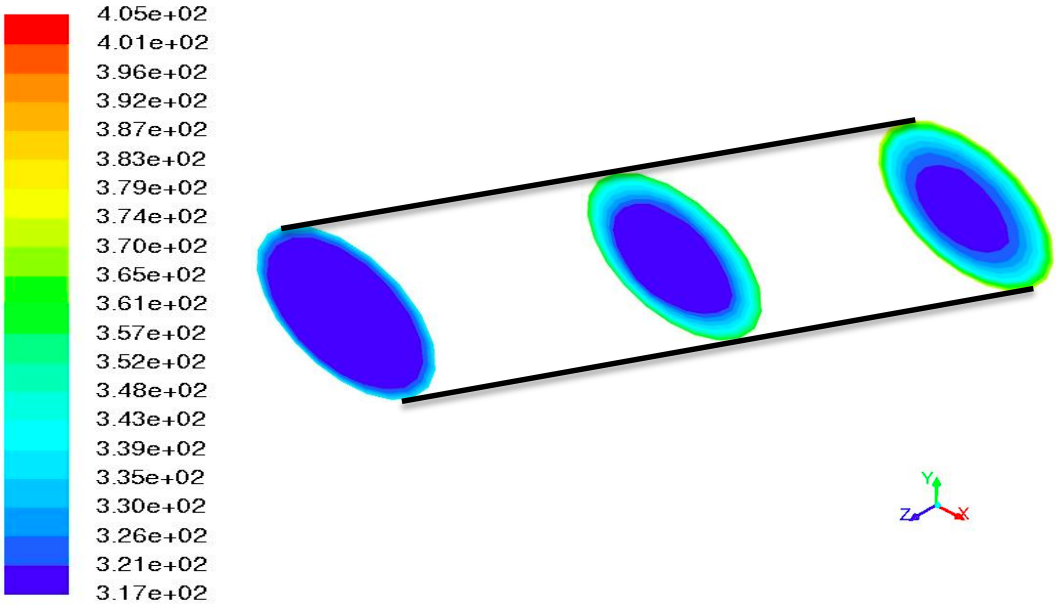

Figure 3.18 Area weighted average temperature of nanofluid at 3 sections of the tube (Z=0, 0.5 and 1) at 40°C and 1% CuO concentration

Table 3.3. Theoretical and experimental results of temperature at different location of the tube at 0.25% CuO concentration at 40°C

Location	**Inlet**	**Middle**	**Outlet**
Theoretical Temperature (°C)	46	55.7	61.8
Experimental Temperature (°C)	43.8	56	60

Table 3.4. Theoretical and experimental results of temperature at different location of the tube at 1% CuO concentration at 40°C

Location	**Inlet**	**Middle**	**Outlet**
Theoretical Temperature (°C)	46.7	54.2	59.8
Experimental Temperature (°C)	44.8	56	59.5

3.2.2.1 Results of Laminar Flow

Particle trajectories at different locations in the tube at CuO concentration of 0.25 and 1% at 40°C are presented in Figures 3.19 and 3.20 respectively. As it is shown in these figures there is almost no particle motion in the radial direction for both the 0.25% and 1% concentrations under laminar flow conditions. Radial position of particles along the tube and momentum boundary layer are shown in Figure 3.21. As it is illustrated there in both cases the particles do not pass the momentum boundary layer. Since the momentum boundary layer does not provide an adequate explanation for the difference in heat transfer coefficient enhancement at 40°C, we decided to focus instead on the thermal boundary layer.

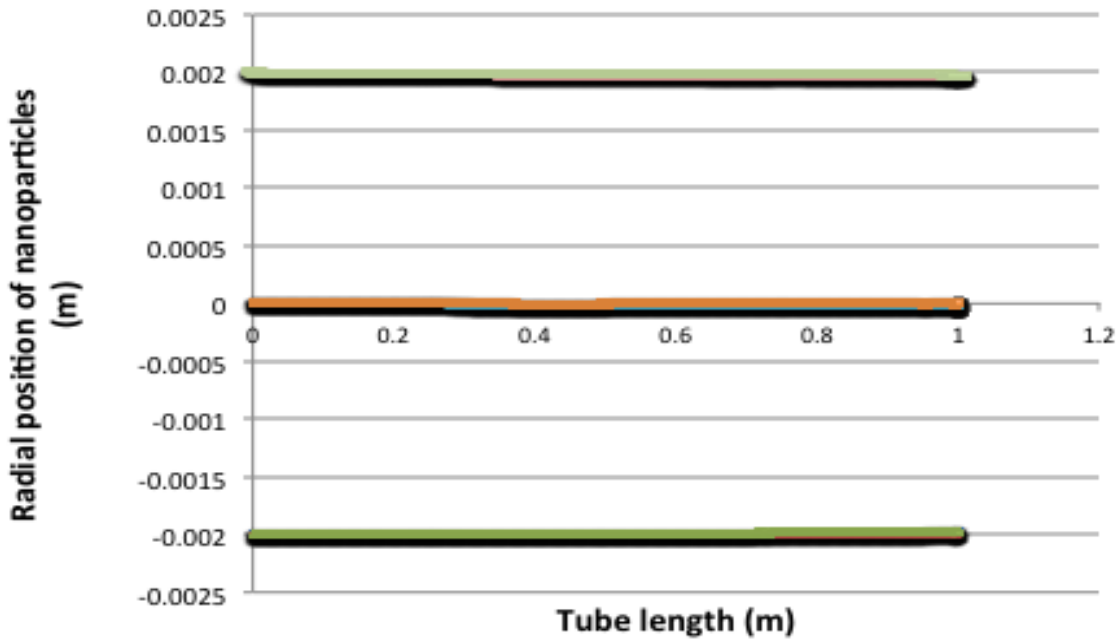

Figure 3.19. Radial position of nanoparticles of CuO/water with 0.25% concentration in laminar (Re=1000) at 40°C

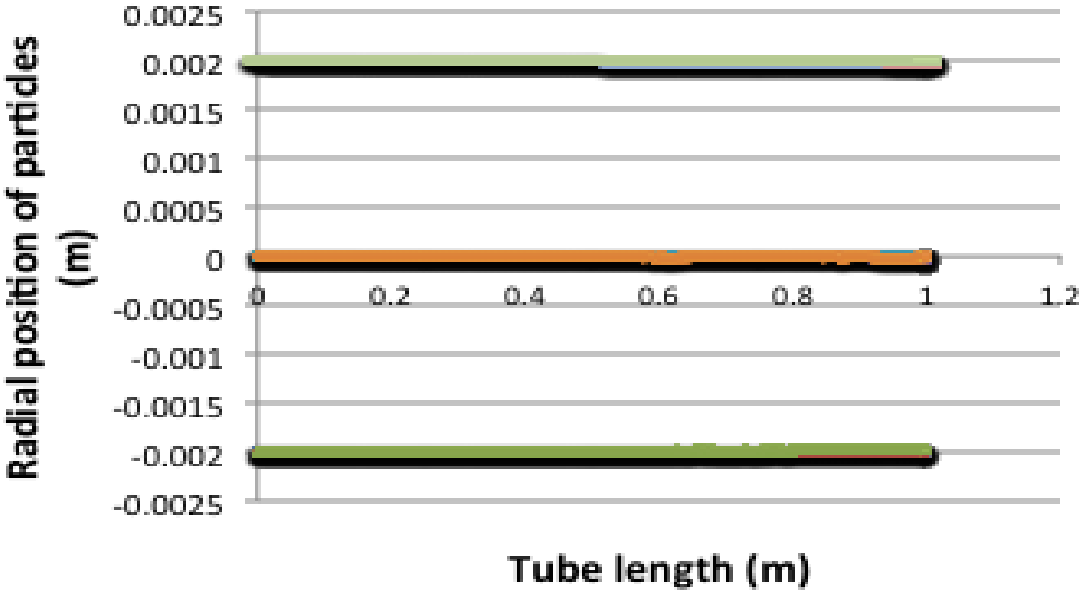

Figure 3.20. Radial position of nanoparticles of CuO/water with 1% concentration in laminar (Re=1000) at 40°C

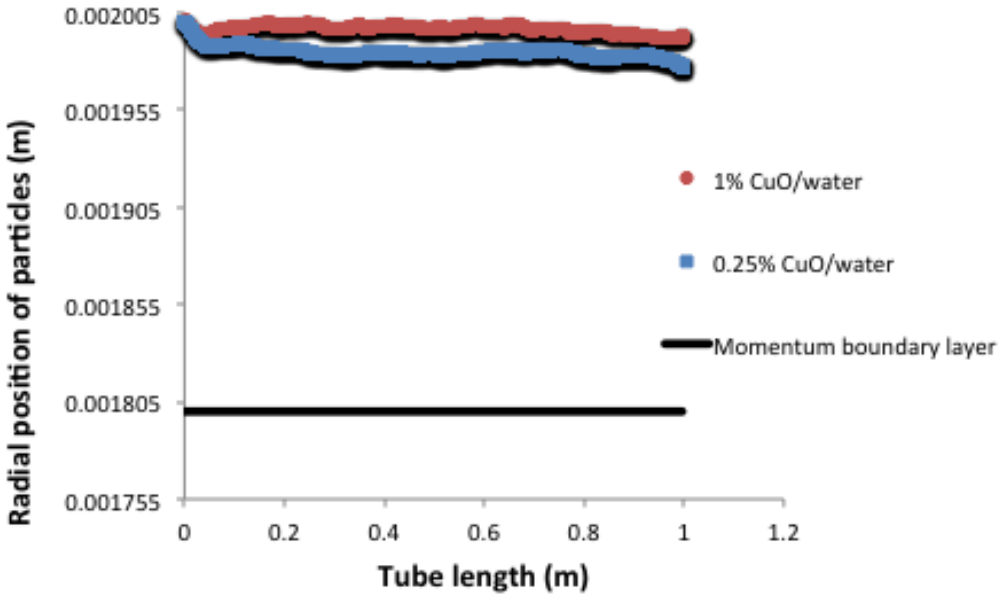

Figure 3.21. Thermal boundary layer and radial position of particles in nanofluids with 0.25 and 1% concentration in laminar flow (Re=1000) at 40°C (the center of the tube is located on the vertical axis at 0)

Much like the momentum boundary layer, the thermal boundary layer is the distance from the wall to a point where the fluid temperature reaches the maximum temperature (in this case wall temperature). This distance is defined normal to the wall, at the point where the flow temperature is 99% of the maximum temperature. The thermal boundary layer and radial position of particles are shown in Figure 3.22.

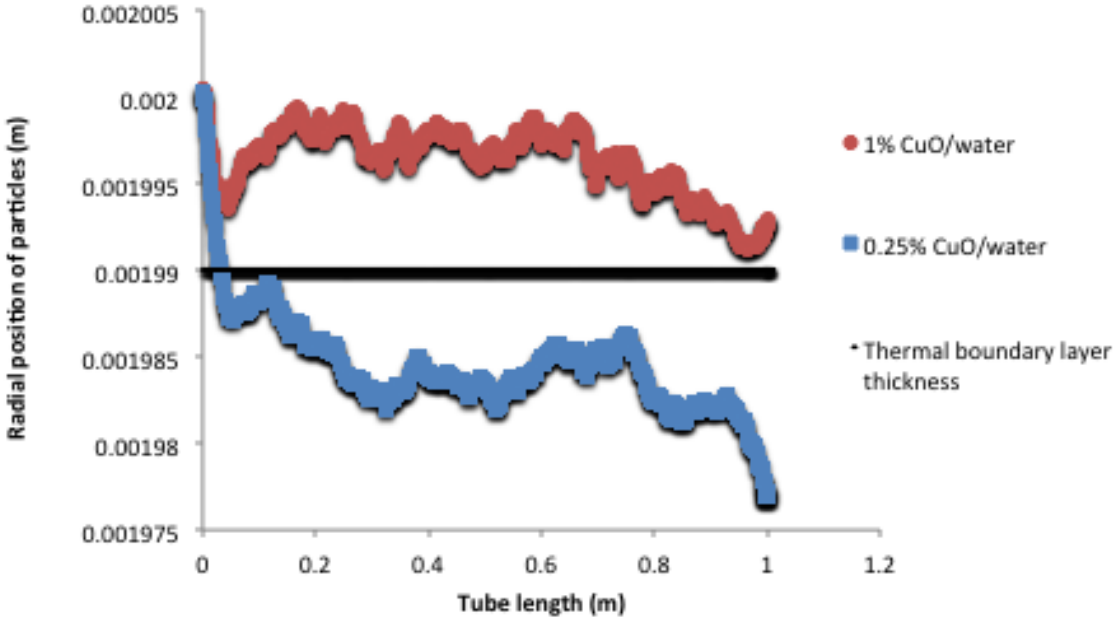

Figure 3.22. Thermal boundary layer and radial position of particles in nanofluids with 0.25 and 1% concentration in laminar flow (Re=1000) at 40°C (the center of the tube is located on the vertical axis at 0)

As is illustrated in Figure 3.22, particles can pass across the thermal boundary layer into the bulk flow of the fluid at the lower CuO concentration (0.25%wt CuO). In this case particles move from the tube wall to the bulk fluid where the temperature gradient between the nanoparticle and the fluid is available for heat transfer. This means that adding CuO nanoparticles could effectively enhance heat transfer within the fluid. At the 1% CuO concentration though, the nanoparticles do not move through boundary layer but they still have motions within boundary layer allowing for fluid contact with the wall, which leads to positive enhancement though they cannot transfer heat the same as 0.25%wt because they could not pass thermal boundary layer. This evidence eventually leads to a higher heat transfer enhancement at lower concentration (0.25%CuO) compared to the higher concentration (1%CuO) at laminar flow regime, the fact that was observed from experimental results which is shown in Figure 3.5.

3.2.2.2 Results of Turbulent Flow

Particle migration along the tube in turbulent flow at the 0.25 and 1% concentrations at 40°C is illustrated in Figures 3.23 and 3.24. In both cases, the particles can cross the entire diameter of the tube and they are well mixed, which is the reason in Figure 3.5 heat transfer enhancement was almost the same at both cases. However, the 0.25% case shows particles do not cover the diameter of the tube as well as the 1% concentration. At 1% particles exit from the tube in a different radial position from their position at the inlet indicating movement across the tube. Particles move into the wall and away from the wall multiple times where they can gather heat from wall and transfer it into fluid constantly. On the other hand, at 0.25% particles do not have nearly the amount of back and forth motion and they exit from nearly the same position they entered the tube. This shows why the 0.25% has decreasing trend with respect to Re, while the 1% has an increasing trend.

An increasing trend of heat transfer enhancement observed for 1% could be addressed by this fact that at laminar flow particle could not move through the boundary layer while in turbulent flow they can easily transfer heat from the wall to the entire of the tube. On the other hand, for 0.25% case particles could move through the boundary layer and they could easily transfer heat from the wall to the center of the tube, while, at turbulent particles accumulate near the wall and they do not move through the entire tube so they could not provide large temperature gradient and they add little to mixing and they could not enhance heat transfer of water. Therefore, we observe a decreasing trend with Re for 0.25%.

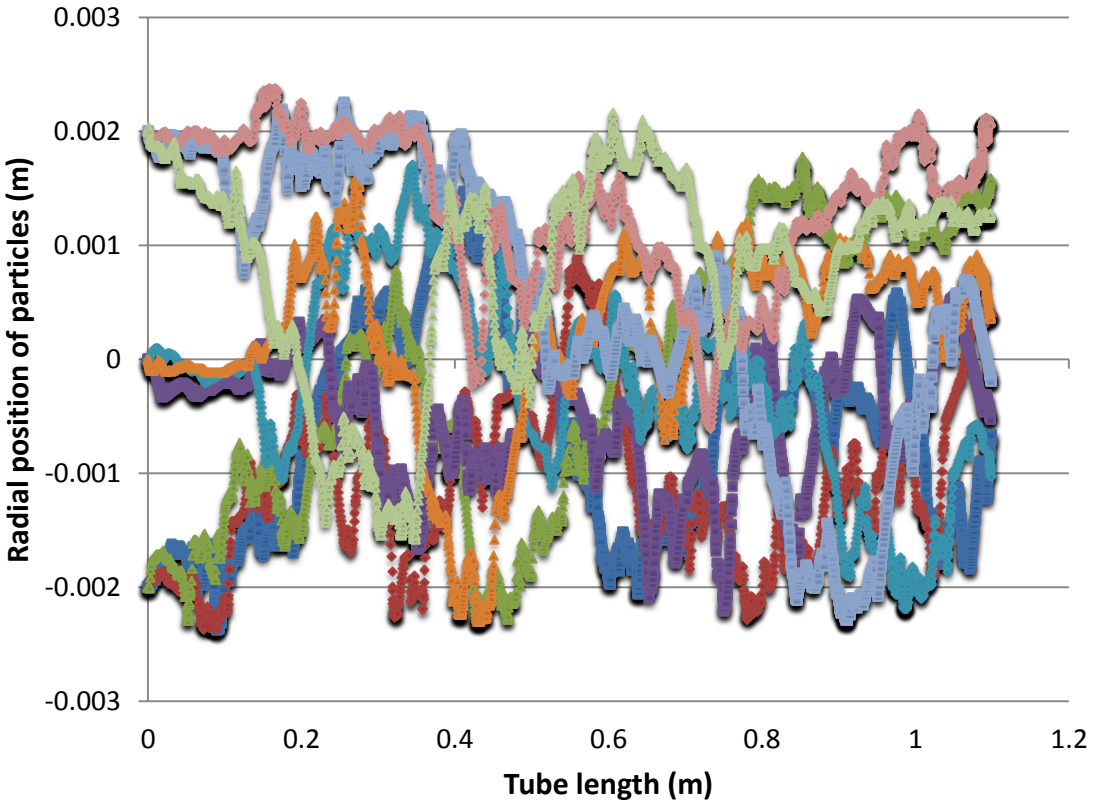

Figure 3.23. Radial position of nanoparticles of CuO/water with 0.25% concentration in turbulent (Re=4000) at 40°C

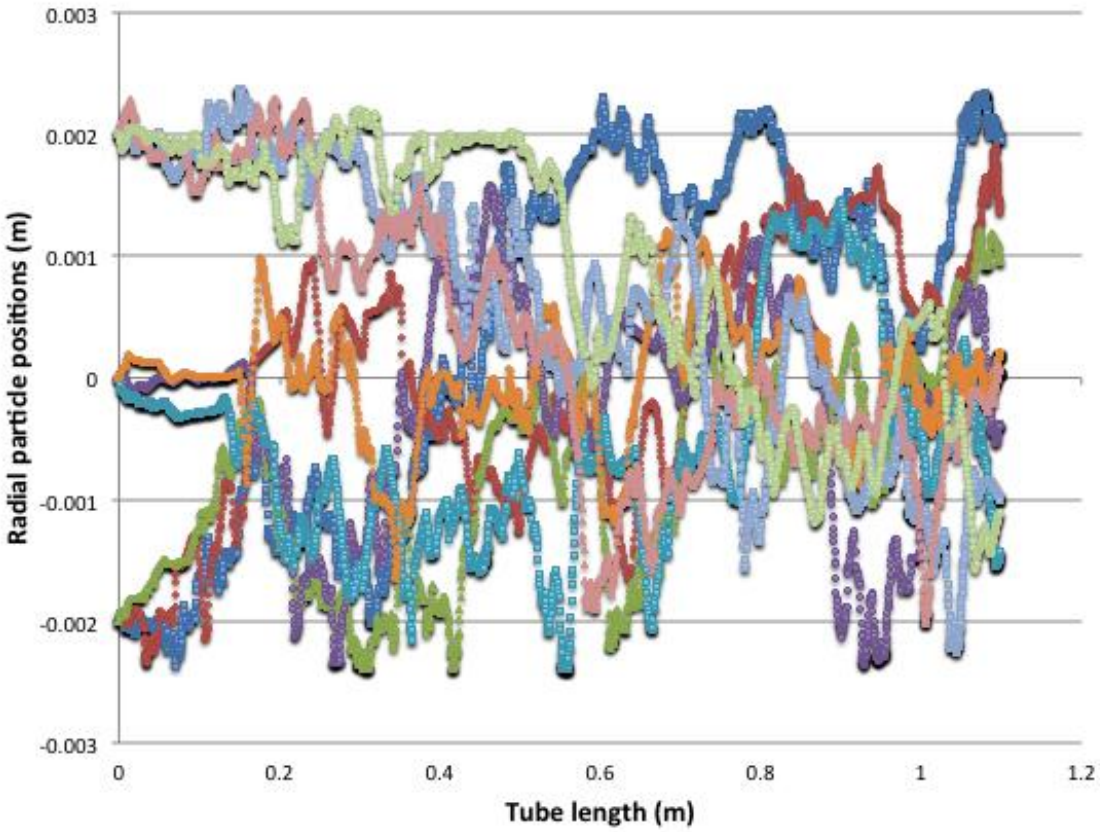

Figure 3.24. Radial position of nanoparticles of CuO/water with 1% concentration in turbulent (Re=4000) at 40°C

So it seems that thermal boundary layer is more important than momentum boundary layer as our system is heat transfer. So we take a look back to 70°C to find out if particles could pass thermal boundary layer at 70°C. The thermal boundary layer at 70°C is calculated the same way for as discussed for 40°C. Figure 3.25 shows the thermal boundary layer and radial position of nanoparticles at 70°C. Figure 3.25 shows that at 1% CuO concentration particles pass thermal boundary layer. This gives the heated particles a better chance to move from the tube wall to the bulk fluid where temperature gradient is available to transfer heat collected from the tube wall into the bulk of fluid effectively enhancing the heat transfer within the fluid. In addition, at 1%wt, particles could pass far away from thermal boundary layer at very beginning of the tube which explain the large enhancement we observe in this case. However, at 0.25% particles could not pass thermal boundary layer and they could not be able to drop heat in bulk

fluid.

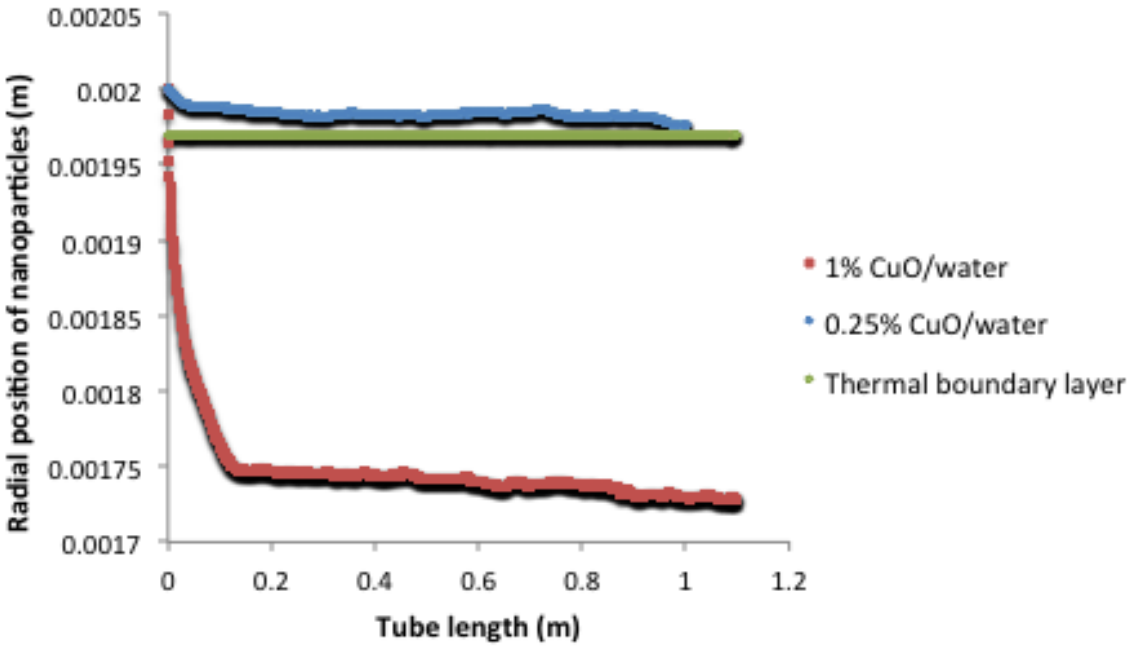

Figure 3.25. Thermal boundary layer and radial position of particles in nanofluids with 0.25 and 1% concentration in laminar flow (Re=1000) at 70°C (the center of the tube is located on the vertical axis at 0)

In overall, the movement of particles away from the boundary layer which provides additional mixing in fluid is the key to enhancing heat transfer under laminar flow conditions. While, under turbulent conditions, the particles are not enhancing mixing/turbulence much beyond what is already present in the base fluid, which would explain why there isn't significant enhancement under those conditions for either weight fraction.

While the simulation results give possible explanations to the heat transfer coefficient enhancements observed in the experimental results, it does not fully explain why the particles move in this manner. To explain the particles motion one should

consider particle motion equation. Several terms are available in particle motion equation to explain particle behavior in these systems beyond just Brownian motion such as drag, Siffman lift, thermophoretic, and gravity forces. Based on our simulation and experimental results it seems that situations that promote Brownian motion and particle-particle interaction like high temperature, low viscosities, turbulent mixing lead to lower enhancements. To have a better understanding of particles motion one should deeply study impact of all forces such as Brownian, gravity, drag, thermophoretic and siffman lift forces to find out their relative importance on particle motion. More likely, one of the forces active within the system, such as the thermophoretic force, is responsible for the initial particle motion and the observed enhancement.

CHAPTER IV

CONCLUSIONS AND FUTURE DIRECTIONS

Conclusions:

The heat transfer coefficient of water and CuO/water nanofluids with CuO concentration of 0.25, 1 and 2%wt at 40, 60 and 70°C were measured experimentally. The results indicate an increasing trend of heat transfer coefficient with increasing Reynolds number for all nanofluids investigated which is not unexpected in cases of convective heat transfer. The heat transfer was further observed to decrease with increasing temperatures at constant particle loading and Re which is in conflict with several previous works that suggest that conditions more conducive to Brownian motion (i.e. higher temperatures) should result in higher heat transfer coefficients.

The heat transfer coefficient does not provide any information regarding nanofluids being more effective that the base fluid. Therefore, heat transfer enhancement at different concentrations of CuO and different temperatures was calculated by taking the ratio of the heat transfer coefficient of the nanofluid to that of the base fluid at specific Re and initial temperatures. The experimental results illustrated that flow rate (Re), particle concentration and temperature are all capable of impacting the enhancement but not in a predictable way.

The experimental results at 60°C show that heat transfer coefficient

enhancement increases initially with concentration from 0.25% to 1%wt. But, as concentration is increased further, from 1% to 2%wt, there is a decrease in the enhancement. Additionally, at all concentration, a decreasing trend of heat transfer coefficient enhancement with respect to Re is observed. This result indicates that it is more beneficial to use nanofluids under laminar flow condition as the enhancement is higher which is similar to the conclusions presented in other works on heat transfer in nanofluids. However, this same trend with respect to Re is not observed at all nanoparticle concentrations for the other temperatures investigated in this work.

At 70°C the CuO/water nanofluid with CuO concentration of 0.25%wt and Reynolds number 1000 was observed to have a 12% enhancement while the 1%wt CuO has a negative enhancement. However, at Reynolds around 6000 both the 0.25% and 1%wt have the same value of enhancement of about 4%. These results indicate that at a concentration of 1%wt, there is a decreasing trend in heat transfer coefficient enhancement with respect to Re while an increasing trend with respect to Re is observed at 0.25%wt.

On the other hand, at 40°C and Re of 1000, the nanofluid with the lower concentration (0.25%wt) has highest enhancement (13%) compared to the 1%wt CuO/water nanofluid which only has a 2% enhancement. Conversely, both cases have the same enhancement (around 8%) at a Reynolds of 4000. This results in exactly the opposite trends that were observed at 70°C, namely that an decreasing trend is observed in enhancement at 0.25% while 1% shows increasing trend with respect to Re. It should be noted that at both temperatures, a decreasing trend in heat transfer coefficient enhancement was observed at the 2%wt nanoparticle concentration.

To further explain the experimentally observed trends in the heat transfer

enhancement of CuO/water nanofluids with respect to nanoparticle concentration and Re we developed a CFD model using an Eulerian-Lagrangian approach to further explain the impact of these variables on the hydrodynamic and thermal parameters of a nanofluid. The geometry for the CFD modelling was set to match the dimensions of the copper tube in the heat exchange section of the experimental system at 1.095 m length and 0.0048 m in diameter. A very fine mesh was used near the wall of the tube while a more coarse mesh was used in the center. This distribution was chosen specifically as it was suspected that particle interactions with the heated wall would be more important than particle interactions in the center of the tube. The total number of nodes within the mesh was set at 263,000 based on a check of the mesh sensitivity.

To validate the model, the residual convergence as well as the convergence of the area weighted average temperature at the outlet of the tube was verified. The theoretical temperature results of the nanofluid at different positions along the length of the tube were then compared with the experimental data from the thermocouples at the same positions along the tube. The temperature results from the simulation match well with the experimental data. These verifications indicate that the model is accurately predicting the behavior of the nanofluids within the heat transfer system.

The CFD model was then used to track particle motion through the tube. Three particles were injected at each of three different positions at the entrance of the tube using a cone injection type. Injection positions were chosen near the top and bottom of the horizontal tube as well as the center of the tube. The simulation results show that in some cases under laminar flow conditions, the particles would move away from the wall and through the thermal boundary layer very close to the entrance of the tube. When compared with the experimental results, it was found that the heat transfer

coefficient enhancement was higher in these cases than for those where the particles remained near the wall within the thermal boundary layer along the entire length of the tube. By moving through the boundary layer and into the bulk flow of the nanofluid, the nanoparticles are able to transfer heat from the wall into the fluid. Additionally, the movement of the particles will lead to a disturbance, or mixing of the fluid in the entrance region. Both of these will contribute to the enhancement of the heat transfer within the system. In all cases for laminar flow, the particles injected in the center of the tube remained in the center for the entire length of the tube.

This initial motion of particles away from the wall at the entrance region of the tube is not directly related to Brownian motion. Once the particles have entered the bulk flow of the fluid under laminar conditions, Brownian motion of the particles can be directly observed and is orders of magnitude smaller than the initial motion through the boundary layer. This suggests that Brownian motion is not related to the enhancement of the heat transfer coefficient. More likely, one of the other forces active within the system, such as the thermophoretic force, is responsible for the initial particle motion and the observed enhancement. Simulations performed where particle-particle interactions were taken into account showed no difference to those performed without particle-particle interactions which suggests that particle-particle interactions are not important within this system. While this is not surprising given the low particle concentrations being used in this work, it also suggests that the impact of Brownian motion within the system is limited.

Based on our experimental and theoretical results at turbulent flow conditions, particles add a little to the mixing and turbulence within the fluid. The simulations show that the particles are constantly able to move effectively from the wall to the center of the tube giving rise to a small amount of enhancement that is observed in the

experimental work. Unfortunately, their motion adds little to the turbulence that already exists within the fluid under these conditions. According to this, the impact of mixing and turbulence in the fluid on heat transfer is more important than the addition of the small concentration of higher thermal conductivity nanoparticles used in this work.

Devices such as high speed microprocessors, laser application apparatus, super conductive magnets and optoelectronics require high heat transfer cooling systems. According to our results, laminar flow should be chosen so that heat transfer coefficient could be effectively enhanced in these systems as the highest enhancements in this work were observed under these conditions. However, it is very important that the nanoparticles pass thermal boundary layer to provide the highest heat transfer enhancement. To ensure that this is the case, simulations of the particle trajectories should be performed based on the exact geometry of the system to ensure that the correct particle concentrations and fluid temperature are used.

Future Directions:

Based on this work, there are a number of avenues of research that still need to be performed, both in terms of experimental and simulation studies. For future experimentation studies, the results from this work and others suggest that the use of nanofluids in laminar flow will results in higher levels of heat transfer enhancement. Changing the geometry of the particle from the spherical 40 nm particles used in this work could lead to some additional insights into the heat transfer process in these systems. As an example, based on previous work, decreasing particle size can lead to larger enhancements possibly due to the increased surface area of the particle contacting the fluid. Additionally, changing particle shape to that of a rod or a plate will allow the particle to interact with the laminar flow field differently than a spherical particle. This will possibly introduce different mixing effects and surface area enhancement effects to the system. Particle material is also of interest as heat transfer enhancement is seemingly tied to the thermal conductivity of the particles. Working with higher thermal conductivity materials, such as Al and Cu could lead to additional enhancements beyond those observed in this work. As the research space is still very large, it is strongly suggested that a design of experiments be completed before performing these experiments so as to limit the time needed to acquire statistically significant data based on the large number of experimental variables that are present within this system.

In future simulation studies, the aim should be focused on explaining the particle

trajectories, especially those that allow the particles to cross the thermal boundary layer. These fundamental studies should look at the different terms in the equation of particle motion to determine which are dominant under the different conditions used in this work. The effect of Brownian, gravity, drag, thermophoretic and siffman lift forces on particle motion should be carefully considered. While there is a suggestion in this work and others that the thermophoretic forces may be important within this system, the other forces cannot be discounted completely. One important aspect observed in this work that may not be fully appreciated in other studies is that particle motion within these systems is not only a function of temperature, but also of particle concentration. Determining the role of both of the factors on each of the forces in the particle motion equation may be the key to discovering how the particles move relative to the thermal boundary layer under laminar conditions and why this changes in seemingly non-predictable ways based on particle concentration and fluid temperature.

Ultimately, these nanofluids must be utilized in commercially relevant systems to demonstrate the possible performance enhancements over the commonly used heat transfer fluids. One possible application would be in the cooling of high speed CPUs and microprocessors. A heat transfer system could be designed and optimized in a simulation environment to take advantage of the nanoparticles within the nanofluid. Additional simulations would need to be performed to demonstrate that the particles are able to break through the thermal boundary layer in the area for highest heat exchange based on the geometry of the system, i.e. flow through a slit with a heated side. Based on the results of the simulation, a demonstration system could be built and tested for use. Initial testing could be performed using a Peltier heater to demonstrate the proof of concept. The final feasibility demonstration could be performed by

modifying the design to work on the CPU of a high end computer system. Such computers are currently cooled using water based systems and could benefit from the heat transfer enhancement offered by a water-based nanofluid.

REFERENCES

[1] Gribbin, J., Richard Feynman: “A Life in Science. Dutton” 170, 1997.

[2] Taniguchi, N., On the Basic Concept of "Nano-Technology". Proc. Intl. Conf. Eng. Tokyo, Part II, Japan Society of Precision Engineering, 1974.

[3] Chopra, A., V. Kundra, and P. Weiser, “National Nanotechnology Initiative Strategic Plan” 2011.

[4] Stephen U.S Choi and J.A Eastman “Enhancing thermal conductivity of fluids with nanoparticles” Energy technology Division and materials science division, Argonne national laboratory, aregonne, IL 60439, 1995.

[5] L. Qiang, X. Yimin, “convective heat transfer and flow characteristics of Cu-water Nanofluid” Science in China, 45, 408-416, 2002.

[6] X. Wang, X. Xu, S.Chio “Thermal Conductivity Of Nanoparticle Fluid Mixture” Journal of Thermophyscis and Heat Transfer, 13 (4), 474-480, 1999.

[7] S. Lee, S. Chio, S. Li “Measuring Thermal Conductivity of Fluids Containing Oxide Nanoparticles” Journal of Heat Transfer, 121, 280-289, 1999.

[8] M. Jala, H. Meisami and M. Pouyagohar, “experimental Study of CuO/Water Nanofluid Effect on Convective Heat Transfer of a Heat Sink” Middle-East Journal of Scientific Research 13 (5), 606-611, 2013.

[9] Sathyanarayanan, P.L. and R. Ramprabhu “Study on the effect of different combinations of engine coolant additives on the heat dissipation rate of radiators” Proceedings of the Institution of Mechanical Engineers Part D, Journal of Automobile Engineering, 2005. 219(D10): p. 1173-1179.

[10] Yu, W., et al., Review and Assessment of Nanofluid Technology for Transportation and Other Applications. 2007.

[11] Praveen K. Namburu, Debendra K. Das, Krishna M. Tanguturi, Ravikanth S. Vajjha “Numerical study of turbulent flow and heat transfer characteristics of nanofluids considering variable properties” International Journal of Thermal Sciences (48) 290–302, 2009.

[12]Wang, X.Q. and A.S. Mujumdar "Heat transfer characteristics of nanofluids: a review" International Journal of Thermal Sciences, 46(1) 1-19, 2007

[13] Xuan, Y. and Q. Li "Heat transfer enhancement of nanofluids" International Journal of Heat and Fluid Flow, 21(1) 58-64, 2000.

[14] W. jiang, C. Shik, J. Nine, H. Afrianto "Heat Transfer Characteristics Of Nanofluid Through Circular Tube" J. Cent.South Univ, 20, 142-148, 2013.

[15] Z. Heris S, N. Esfahany M, " Experimental Investigation Of Convective Heat Transfer Of Al2O3/Water Nanofluid In Circular Tube" International Journal of Heat and Fluid Flow, 28(2): 203–210. 2007.

[16] Z. Heris S, M. Esfahany M, "Investigation Of Cuo/Water Nanofluid Laminar Convective Heat Transfer through a Circular Tube "Journal of Enhanced Heat Transfer" 279-289, 2006.

[17] Bucak, S. "Importance Of Defining When Applying" Chemical Engineering & Process Technology, 2(1) 2011.

[18] Jang, S.P. and S.U.S. Choi "Effects Of Various Parameters On Nanofluid Thermal Conductivity" Journal of Heat Transfer-Transactions of the Asme, 129(5) 617-623, 2007.

[19] Shaikh, S., K. Lafdi, and R. Ponnappan "Thermal Conductivity Improvement In Carbon Nanoparticle Doped PAO Oil: An Experimental Study" Journal of Applied Physics, 101(6) 1-8, 2007.

[20] Xie, H., et al. "Thermal Conductivity Enhancement of Suspensions Containing Nanosized Alumina Particles." Journal of Applied Physics, 91, 4568-4572, 2002.

[21]Wen, D.S. and Y.L. Ding "Experimental Investigation Into Convective Heat Transfer Of Nanofluids At The Entrance Region Under Laminar Flow Conditions" International Journal of Heat and Mass Transfer, 47, 5181-5188, 2004.

[22] Hong, T.K., H.S. Yang, and C.J. Choi "Study Of The Enhanced Thermal Conductivity Of Fe Nanofluids" Journal of Applied Physics, 97(6) 2005.

[23] Masuda, H., et al. "Alteration of Thermal Conductivity and Viscosity of Liquid by Dispersing Ultra-Fine Particles" Netsu Bussei, 7, 227-233, 1993.

[24] Das, S.K., et al., "Temperature Dependence Of Thermal Conductivity Enhancement For Nanofluids" Journal of Heat Transfer-Transactions of the Asme, 125 (4), 567-574, 2003.

[25] Wen, D.S. and Y.L. Ding "Formulation Of Nanofluids For Natural Convective Heat Transfer Applications" International Journal of Heat and Fluid Flow, 26(6) 855-864, 2005.

[26] Li, C.H. and G.P. Peterson "Experimental Investigation Of Temperature And Volume

Fraction Variations On The Effective Thermal Conductivity Of Nanoparticle Suspensions (Nanofluids)" Journal of Applied Physics, 99(8) 2006.

[27] Hong, K.S., T.K. Hong, and H.S. Yang, "Thermal Conductivity Of Fe Nanofluids Depending On The Cluster Size Of Nanoparticles" Applied Physics Letters, 88(3) 2006.

[28] Xie, H., et al., "Thermal Conductivity of Suspensions Containing Nanosized SiC Particles. International Journal of Thermophysics and Heat Transfer" 23, 571-580, 2002.

[29] Xie, H.Q., et al., "Dependence Of The Thermal Conductivity Of Nanoparticle-Fluid Mixture On The Base Fluid" Journal of Materials Science Letters, 21(19) 1469-1471, 2002.

[30] Ding, Y.L., et al., "Heat Transfer Of Aqueous Suspensions Of Carbon Nanotubes (CNT Nanofluids)" International Journal of Heat and Mass Transfer, 49(1-2) 240-250, 2006.

[31] Eastman, J.A., et al., "Anomalously Increased Effective Thermal Conductivities Of Ethylene Glycol-Based Nanofluids Containing Copper Nanoparticles" Applied Physics Letters, 78(6): p. 718-7202001.

[32] Assael, M.J., et al., "Thermal Conductivity Enhancement In Aqueous Suspensions Of Carbon Multi-Walled And Double-Walled Nanotubes In The Presence Of Two Different Dispersants" International Journal of Thermophysics, 26(3): p. 647-664, 2005.

[33] Kan Liu "Measurement Of Heat Transfer Mechanisms In Oil Based Nanofluids" Ph.D. Dissertation, University of Louisville, 2011.

[34] C. T. Nguyen, G. Roy, C. Gauthier, N. Galanis " Heat Transfer Enhancement Using Al2O3-Water Nanofluid For Electronic Liquid Cooling System" Applied Thermal Engineering, 28(8),1501–1506, 2008.

[35] M. Heyhat, F. Kowsary, A.M. Rashidi, S. Alem Varzane Esfehani, A. Amrollahi "Experimental Investigation Of Turbulent Flow And Convective Heat Transfer Characteristics Of Alumina Water Nanofluids In Fully Developed Flow Regime" International Communications in Heat and Mass Transfer, 39(8), 1272–1278, 2012.

[36] Putra, N., W. Roetzel, and S.K. Das "Natural convection of nano-fluids' Heat and Mass Transfer, 39(8-9): p. 775-784, 2003.

[37] B.C. Pak, Y.I. Cho "Hydrodynamic And Heat Transfer Study Of Dispersed Fluids With Submicron Metallic Oxide Particles" Experimental Heat Transfer, 11(2), 151-170, 1998.

[38] S.M. Fotukian, M. Nasr Esfahany " Experimental Study Of Turbulent Convective Heat Transfer And Pressure Drop Of Dilute Cuo/Water Nanofluid Inside A Circular Tube" International Communications In Heat And Mass Transfer, 37(2), 214–219, 2010.

[39] Li, Q. and Y.M. Xuan "Experimental Investigation Of Transport Properties Of Nanofluids" Heat Transfer Science & Technology. Higher Education Press, p. 757-762,

2000.

[40] Xuan, Y.M. and Q. Li “Investigation On Convective Heat Transfer And Flow Features Of Nanofluids” Journal of Heat Transfer-Transactions of the Asme, 125(1): p. 151-155, 2003.

[41] A. Akbarnia , A. Behzadmehr “Numerical Study Of Laminar Mixed Convection Of A Nanofluid In Horizontal Curved Tube” Appl. Thermal Sci. 27, 1327–1337, 2007.

[42] S. Mirmasoumi , A. Behzadmehr “Numerical Study Of Laminar Mixed Convection Of A Nanofluid In A Horizontal Tube Using Two-Phase Mixture Model” Applied Thermal Engineering 28, 717–727, 2008.

[43] Habib Aminfar, Roghayyeh Motallebzadeh “Investigation of the Velocity Field and Nanoparticle Concentration Distribution of Nanofluid Using Lagrangian-Eulerian Approach” Journal of Dispersion Science and Technology, 33:155–163, 2012.

[44] P.Kumar “A CFD Study of Heat Transfer Enhancement in Pipe Flow with Al_2O_3 Nanofluid” World Academy of Science, Engineering and Technology, 5, 09-23, 2011.

[45] Kai Jin “Modeling Nano-Particle Migration in Pipe Flow through Eulerian-Lagrangian Approach” M.s. Thesis Lehigh University, 2011.

[46] Zhou LP, Wang BX, Peng XF, Du XZ, Yang YP “On The Specific Heat Capacity Of Cuo Nanofluid” Adv Mech Eng, 1-4, 2010.

[47] Buongiorno J. “Convective Transport In Nanofluids” Journal of Heat Transfer, 128:240-250, 2006.

[48] A. J. Chorin. "Numerical solution of navier-stokes equations". Mathematics of Computation. 22. 745–762. 1968.

[49] ANSYS Fluent Theory Guide.

[50] P. A. Cundall and O. D. L. Strack. "A Discrete Numerical Model for Granular Assemblies". Geotechnique. 29. 47–65. 1979.

[51] Li A and Ahmadi G “Deposition Of Aerosols On Surfaces In A Turbulent Channel Flow” Int. J. Eng. Sci. 31 435–51, 1993.

[52] P. G. Saffman "The Lift on a Small Sphere in a Slow Shear Flow" J.Fluid Mech. 22. 385–400, 1965.

[53] P. Spalart and S. Allmaras. "A One-Equation Turbulence Model For Aerodynamic Flows". Technical Report AIAA-92-0439. American Institute of Aeronautics and Astronautics. 1992.

APPENDICES

OVERVIEW OF USING THE SOLVER

1.1 Over View of Flow Solver

In ANSYS FLUENT, two solver technologies are available:

- pressure-based
- density-based

Both solvers can be used for a broad range of flows, but in some cases one formulation may perform better (i.e., yield a solution more quickly or resolve certain flow features better) than the other. The difference between pressure-based and density-based approaches is in the way that the continuity, momentum, and (where appropriate) energy and species equations are solved.

The pressure-based solver traditionally has been used for incompressible and mildly compressible flows. While, the density-based approach was originally designed for high-speed compressible flows. Both approaches are now applicable to a broad range of flows (from incompressible to highly compressible), but the origins of the density-based formulation may give it an accuracy advantage over the pressure-based solver for high-speed compressible flows. Figure 1 shows how to choose the solver from general task page.

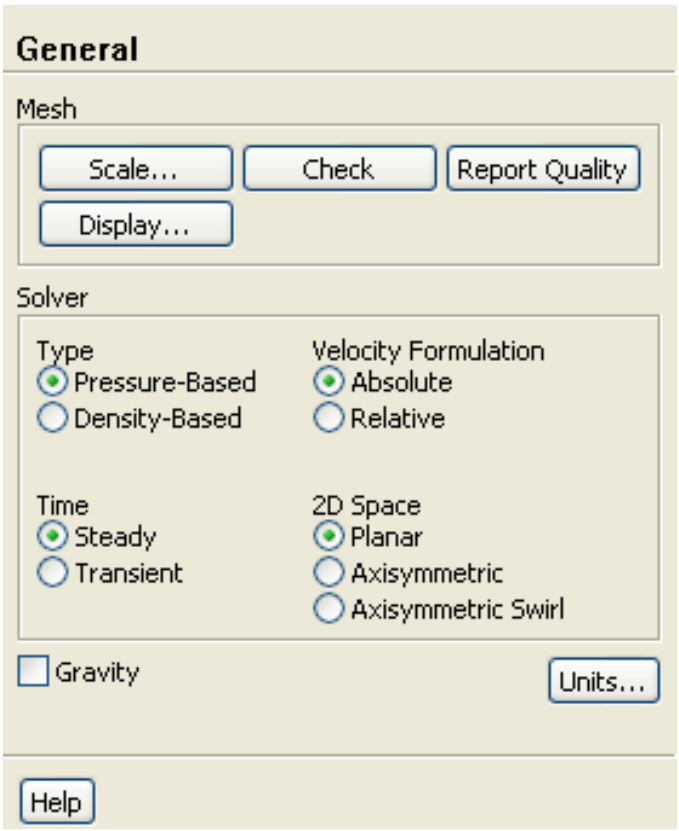

Figure 1. The General Task Page

Two algorithm exist under the density-based solver: implicit and explicit. The density-based explicit and implicit formulations solve the equations for additional scalars (e.g., turbulence or radiation quantities) sequentially. The implicit and explicit density-based formulations differ in the way that they linearize the coupled equations.

A converged steady-state solution can be obtained much faster using the implicit formulation rather than the explicit formulation because of the broader stability characteristics of the implicit formulation. However, the implicit formulation requires more memory than the explicit formulation.

The pressure-based solver employs an algorithm which belongs to a general class

of methods called the projection method [48]. In the projection method, the constraint of mass conservation (continuity) of the velocity field is achieved by solving a pressure (or pressure correction) equation. The pressure equation is derived from the continuity and the momentum equations in such away that the velocity field, corrected by the pressure, satisfies the continuity. As the governing equations are nonlinear and coupled to one another, the solution process involves iterations wherein the entire set of governing equations is solved repeatedly until the solution converges.

Two formulations also exist under the pressure-based solver in ANSYS FLUENT: a segregated algorithm and a coupled algorithm. In the segregated algorithm the governing equations are solved sequentially, segregated from one another, while in the coupled algorithm the momentum equations and the pressure-based continuity equation are solved in a coupled manner. In general, the coupled algorithm significantly improves the convergence speed over the segregated algorithm; however, the memory requirement for the coupled algorithm is more than the segregated algorithm [49].

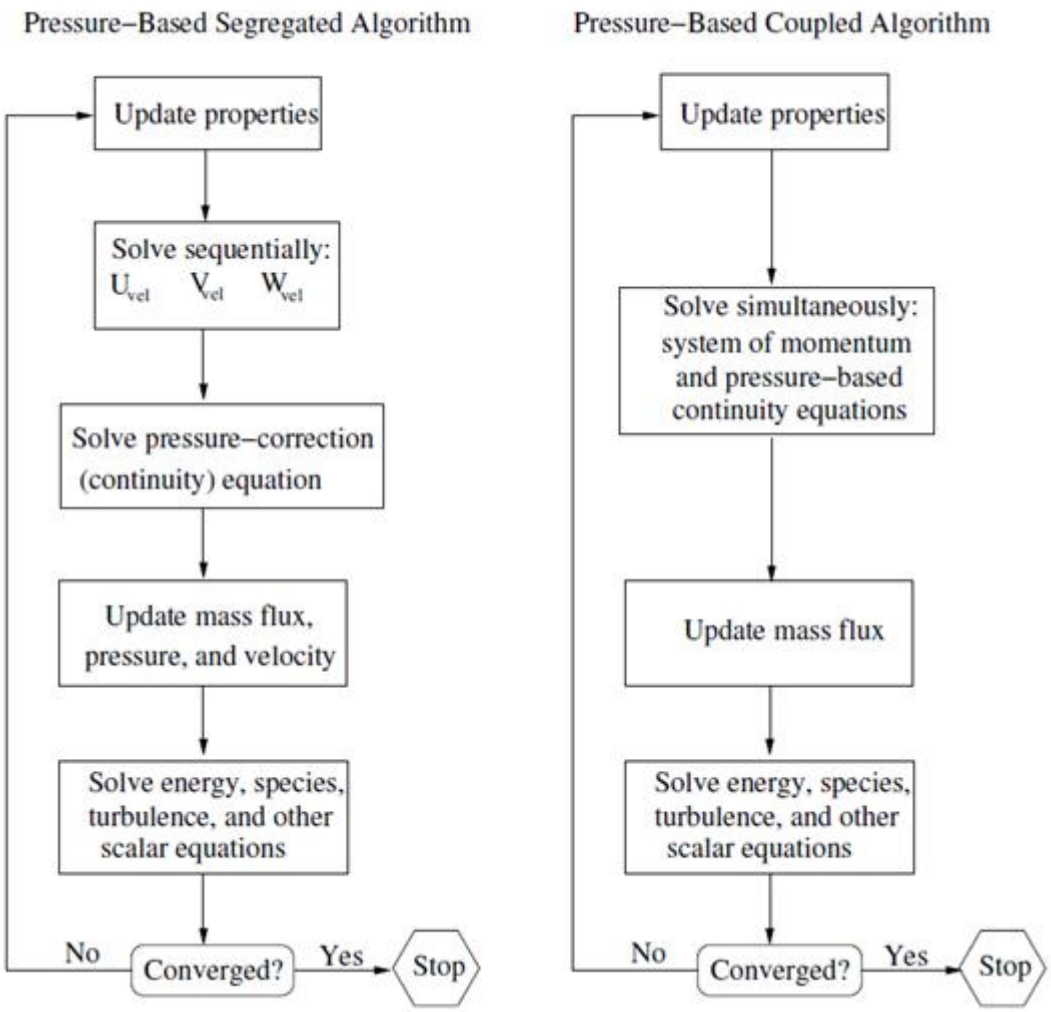

Figure 2. Overview of the Pressure-Based Solution Methods [49]

When selecting a solver and an algorithm one must consider the following issues:

- The model availability for a given solver.
- Solver performance for the given flow conditions.
- The size of the mesh under consideration and the available memory on your machine. This issue could be an important factor in deciding whether to use an explicit or implicit formulation when the

density-based solver is selected, or to use a segregated or coupled algorithm when the pressure-based solver is selected.

The following two lists highlight the model that can be used for each solver (Note that the pressure-based solver provides several physical models or features that are not available with the density-based solver):

Cavitation model

Volume-of-fluid (VOF) model

Multiphase mixture model

Eulerian multiphase model

Non-premixed combustion model

Premixed combustion model

Partially premixed combustion model

Composition PDF transport model

Soot model

Rosseland radiation model

Melting/solidification model

Shell conduction model

Floating operating pressure

Fixed variable option

Physical velocity formulation for porous media

Specified mass flow rate for streamwise periodic flow

The following features are available with the density-based solver, but not with the pressure-based solver:

• Real gas models (User-defined and NIST)

• Non-reflecting boundary conditions

• Wet steam multiphase model

1.2 Overview of Physical Models in ANSYS Fluent

ANSYS Fluent provides comprehensive modeling capabilities for a wide range of incompressible and compressible, laminar and turbulent fluid flow problems. Steady-state or transient analyses can also be performed. In ANSYS Fluent, a broad range of mathematical models for transport phenomena (like heat transfer and chemical reactions) is combined with the ability to model complex geometries.

Various useful features are provided in ANSYS to permit modeling of fluid flow and related transport phenomena in industrial equipment and processes. For example, porous media, lumped parameter (fan and heat ex- changer), streamwise-periodic flow and heat transfer, swirl, and moving reference frame models.

ANSYS Fluent provides very useful models such as the volume-of-fluid (VOF), mixture, and Eulerian models, as well as the discrete phase model (DPM). The DPM performs Lagrangian trajectory calculations for dispersed phases (particles, droplets, or bubbles), including coupling with the continuous phase. The basic physical models ANSYS provides for single phase and multiple phase flows. Examples of multiphase flows include channel flows, sprays, sedimentation, separation, and cavitation.

1.2.1 Approaches to Multiphase Modeling

Advances in computational fluid mechanics have provided the basis for further insight into the dynamics of multiphase flows. In addition to solving transport equations for the continuous phase, ANSYS FLUENT allows you to simulate a discrete second phase in a Lagrangian frame of reference. This second phase consists of spherical particles (which may be taken to represent solid particles, droplets or bubbles) dispersed in the continuous phase. ANSYS FLUENT computes the trajectories of these discrete phase entities, as well as heat and mass transfer to/from them. The coupling between the phases and its impact on both the discrete phase trajectories and the continuous phase flow can be included.

ANSYS FLUENT provides the following discrete phase modeling options:

- Calculation of the discrete phase trajectory using a Lagrangian formulation that includes the discrete phase inertia, hydrodynamic drag, and the force of gravity, for both steady and unsteady flows

- Prediction of the effects of turbulence on the dispersion of particles due to turbulent eddies present in the continuous phase

- heating/cooling of the discrete phase
- vaporization and boiling of liquid droplets
- combusting particles, including volatile evolution and char combustion to simulate coal combustion
- optional coupling of the continuous phase flow field prediction to the discrete phase calculations
- droplet breakup and coalescence
- consideration of particle/particle collisions and voidage of discrete phase

Currently two approaches for the numerical calculation of multiphase flows are available, the Euler-Lagrange approach and the Euler-Euler approach. These two approches discussed in the next section.

1.2.1.1 The Euler-Euler Approach

In the Euler-Euler approach, the different phases are considered mathematically as interpenetrating continua. The concept of phasic volume fraction is introduced here as the volume of a phase cannot be occupied by the other phases,. These volume fractions are assumed to be continuous functions of space and time and their sum is equal to one. Conservation equations for each phase are derived to obtain a set of equations, which have similar structure for all phases. These equations are closed by providing constitutive relations that are obtained from

empirical information, or, in the case of granular flows , by application of kinetic theory.

Three different Euler-Euler multiphase models are available: the volume of fluid (VOF) model, the mixture model, and the Eulerian model.

- The VOF Model

The VOF model is a surface-tracking technique that can be used for a fixed Eulerian mesh. It is designed for two or more immiscible fluids where the position of the interface between the fluids is of interest. In the VOF model, a single set of momentum equations is shared by the fluids, and the volume fraction of each of the fluids in each computational cell is tracked throughout the domain. Applications of the VOF model include stratified flows, free-surface flows, filling, sloshing, the motion of large bubbles in a liquid, the motion of liquid after a dam break, the prediction of jet breakup (surface tension), and the steady or transient tracking of any liquid-gas interface.

- The Mixture Model

The mixture model is a techniqe applied to two or more phases (fluid or particulate). The phases are treated as interpenetrating continua as in the Eulerian model. The mixture model solves for the mixture momentum equation and prescribes relative velocities to describe the dispersed phases. Applications of the mixture model include particle-laden flows with low loading, bubbly flows, sedimentation , and cyclone separators.

- The Eulerian Model

The Eulerian model is the most complex of the multiphase models in ANSYS Fluent. It solves a set of momentum and continuity equations for each phase. Coupling is achieved through the pressure and interphase exchange coefficients. The manner in which this coupling is handled depends upon the type of phases involved; granular (fluid-solid) flows are handled differently than nongranular (fluid-fluid) flows. For granular flows, the properties are obtained from application of kinetic theory. Momentum exchange between the phases is also dependent upon the type of mixture being modeled. ANSYS Fluent's user-defined functions allow to customize the calculation of the momentum exchange. Applications of the Eulerian multiphase model include bubble columns, risers, particle suspension, and fluidized beds.

1.2.2 The Euler-Lagrange Approach

The Lagrangian discrete phase model in ANSYS Fluent follows the Euler-Lagrange approach. In Euler- Lagrange approach the dispersed phase is not considered as the continuum phase. The fluid phase is treated as a continuum by solving the Navier-Stokes equations, while the dispersed phase is solved by tracking a large number of particles, bubbles, or droplets through the calculated flow field. The dispersed phase can exchange momentum, mass, and energy with the fluid phase.

This approach is made considerably simpler when particle-particle interactions can be neglected, and this requires that the dispersed second phase occupies a low volume fraction, even though high mass loading is acceptable. The particle or droplet trajectories

are computed individually at specified intervals during the fluid phase calculation. This makes the model appropriate for the modeling of spray dryers, coal and liquid fuel combustion, and some particle-laden flows, but inappropriate for the modeling of liquid-liquid mixtures, fluidized beds, or any application where the volume fraction of the second phase cannot be neglected and particle-particle interaction is important. For these cases, particle-particle interactions can be included using the Discrete Element Model, which is discussed in the next section.

1.2.2.1 Discrete Element Method Collision Model

ANSYS Fluent has the option of using the discrete element method (DEM) as part of the DPM capability.

The discrete element method is suitable where particle- particle interaction is important. Note that interaction with the fluid flow may or may not be important. The DPM capabilities allow you to simulate moving particles as moving mass points, where abstractions are used for the shape and volume of the particles. Note that the details of the flow around the particles (for example, vortex shedding, flow separation, boundary layers) are neglected. Using Newton's second law, the governing equation of particle motion defined as:

$$m\frac{d\vec{v}}{dt} = \vec{F}_{drag} + \vec{F}_{\Pr essure} + \vec{F}_{virtual\_mass} + \vec{F}_{gravitation} + \vec{F}_{other}$$
$$\frac{dx}{dt} = \vec{v} \qquad (1)$$

The DEM implementation is based on the work of Cundall and Strack [50] and represents the forces that result from the collision of particles.

These forces then enter through the other forces term in Equation 1. The forces from the particle collisions are determined by the deformation, which is measured as the overlap between pairs of spheres (see Figure 3.) or between a sphere and a boundary. Equation 1 is integrated over time to capture the interaction of the particles, using a time scale for the integration that is determined by the rigidity of the materials. [49]

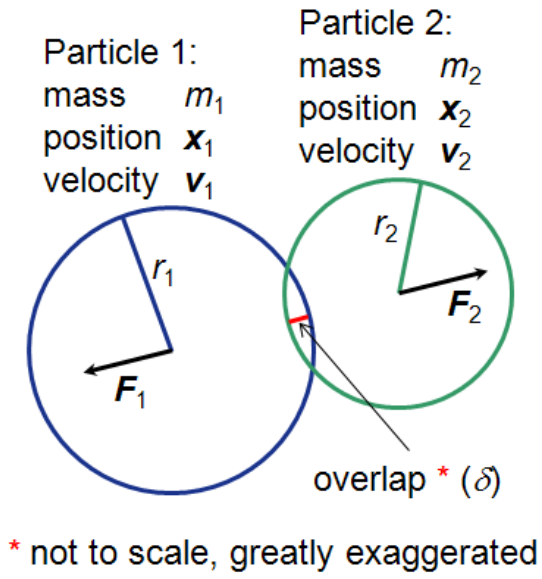

Figure 3. Collisions of particles (Particles Represented by Spheres)

The following collision force laws are available:

- spring
- spring-dashpot
- friction

See ANSYS fluent theory user guide for detailed definition of each low [49].

The size of the spring constant of the normal contact force for a given collision pair should at least satisfy the condition that for the biggest parcels in that collision pair and the highest relative velocity, the spring constant should be high enough to make two parcels in a collision recoil with a maximum overlap that is not too large compared to the parcel diameter. The value of the spring constant (k) can be estimated using the following equation:

$$k = \frac{\rho u^2}{3\varepsilon_D^2} Dr \qquad (2)$$

where D is the parcel diameter, ρ is the particle mass density, v is the relative velocity between two colliding particles, and ε_D is the fraction of the diameter for allowable overlap [49].

1.3 Particle Tracking in Laminar Flow by Eulerian-Lagrangian Method

In this part the particle tracking theory in Eulerian-Lagrangian approach is discussed. Eulerian-Lagrangian approach is where only the main fluid is treated as a continuum, using Eulerian description. The governing equations for the main fluid phase are Navier-Stokes equations, and they are solved by numerical method such as finite difference, finite volume or finite element. However, the dispersed particles are tracked by using the Lagrangian description, and particles can exchange momentum, mass, and energy with the main fluid phase.

1.3.1 Coupling Between the Discrete and Continuous Phases

Discrete phase patterns could be predicted based on a fixed continuous phase flow field which called an uncoupled approach or “one-way coupling”, or you can include the effect of the discrete phase on the continuum which called a coupled approach or “two-way coupling”.

As the trajectory of a particle is computed, ANSYS Fluent keeps track of the heat, mass, and momentum gained or lost by the particle stream that follows that trajectory and these quantities can be incorporated in the subsequent continuous phase calculations. Thus, while the continuous phase always impacts the discrete phase, the effect of the discrete phase on the continuum can also be incorporated. This two-way coupling, where the continuum phase can affect the behavior of discrete phase (particles), and vice versa, is accomplished by alternately solving the discrete and continuous phase equations until the solutions in both phases have stopped changing. It should be mentioned that no interchange terms are computed for particles defined as massless, where the discrete phase trajectories have no impact on the continuum.

1.3.2 Momentum Exchange

The momentum transfer from the continuous phase to the discrete phase is computed in ANSYS Fluent by examining the change in momentum of a particle as it passes through each control volume in the ANSYS Fluent model. This momentum change is computed as follow:

$$F = \sum \left(\frac{18 \mu C_D R_e}{\rho_p d_p^2 24} \left(u_p - u \right) + F_{other} \right) \dot{m}_p \Delta t \qquad (3)$$

μ = viscosity of the fluid
ρ_p = density of the particle
d_p = diameter of particle
R_e = relative Reynolds number
u_p = velocity of the particle
u = velocity of the fluid
C_D = drag coefficient
$\dot{m}_p$ = mass flow rate of the particles
Δt = time step
F_{other} = other interaction forces

The momentum exchange should be calculated and passed to the momentum equation of the continuum as an additional momentum source term.

1.3.3 Heat Exchange

The heat transfer from the continuous phase to the discrete phase is computed in ANSYS Fluent by examining the change in thermal energy of a particle as it passes through each control volume in the ANSYS Fluent model which is computed as:

$$Q = \frac{\dot{m}_{p,0}}{m_{p,0}}\left[\left(m_{p_{in}} - m_{p_{out}}\right)\left[-H_{lat_{ref}} + H_{pyrol}\right] - m_{p_{out}}\int_{T_{ref}}^{T_{P_{out}}} c_{p_p}\, dT + m_{p_{in}}\int_{T_{ref}}^{T_{Pin}} c_{p_p}\, dT\right] \tag{4}$$

$\dot{m}_{p,0}$ = initial mass flow rate of the particle injection (kg/s)
$m_{p,0}$ = initial mass of the particle (kg)
$m_{p_{in}}$ = mass of the particle on cell entry (kg)
$m_{p_{out}}$ = mass of the particle on cell exit (kg)
c_{p_p} = heat capacity of the particle (J/kg-K)
H_{pyrol} = heat of pyrolysis as volatiles are evolved (J/kg)
$T_{p_{in}}$ = temperature of the particle of cell entry (K)
$T_{p_{out}}$ = temperature of the particle of cell exit (K)
T_{ref} = reference temperature of enthalpy (K)
$H_{lat_{ref}}$ = latent heat at reference conditions (J/kg)

1.3.4 Mass Exchange

The mass transfer from the discrete phase to the continuous phase is computed in ANSYS Fluent by examining the change in mass of a particle as it passes through each control volume in the ANSYS Fluent model which is computed as:

$$M = \frac{\Delta m_p}{m_{p,0}} \dot{m}_{p,0} \tag{5}$$

This mass exchange term will be passed to the continuous equation of continuum as a mass source term, so it will finally affect the continuity solution of the fluid.

1.4 Equations of Motion for Particles

1.4.1 Particle Force Balance

As it was mentioned in previous sections ANSYS Fluent predicts the trajectory of a discrete phase particle by integrating the force balance on the particle, which is written in a Lagrangian reference frame. This force balance equates the particle inertia with the forces acting on the particle, and can be written as

$$\frac{d\vec{u}_p}{dt} = F_D(\vec{u} - \vec{u}_p) + \frac{\vec{g}(\rho_p - \rho)}{\rho_p} + \vec{F} \tag{6}$$

where F is the sum of other forces acted on particle (such as Brownian force and gravity) and $F_D(u\text{-}u_P)$ is the drag force per unit particle mass and is defined as:

$$F_D = \frac{18m}{r_p d_p^2} \frac{C_D R_e}{24} \tag{7}$$

In this equation C_D is the drag coefficient, μ is the molecular viscosity of base fluid, ρ is density of the fluid, ρ_P is the density of particle, d_P is the particle diameter, and Re is the relative Reynolds Number

$$R_e = \frac{\rho d_p \left| \vec{u}_p - \vec{u} \right|}{\mu} \tag{8}$$

Here, u is the fluid phase velocity, u_P is the particle velocity, μ is the molecular viscosity of the fluid, ρ is the fluid density, ρ_P is the density of the particle, and d_P is the particle diameter.

1.4.1 Other Forces

Equation 6 includes additional forces (F) in the particle force balance that can be important under special circumstances. These additional forces are listed below:

- Virtual Mass Force

Virtual mass force is the force required to accelerate the fluid surrounding the particle. The virtual mass and pressure gradient forces are not important when the density of the fluid is much lower than the density of the particles as is the case for liquid/solid particles in gaseous flows. For values of approaching unity, the Virtual Mass and Pressure Gradient forces become significant and it is recommended that they be included when the density ratio is greater than 0.1.

- Forces in Moving Reference Frames

The additional force term, F, in Equation 6 also includes forces on particles that

arise due to rotation of the reference frame. These forces are related to the modeling flows in moving frames of reference. In our systems this force is not available.

- Thermophoretic Force

ANSYS Fluent can optionally include a thermophoretic effect on particles in the additional Force term. Thermophoresis force occurs when small particles suspended in a fluid that has a temperature gradient experience a force in the direction opposite to that of the gradient.

- Brownian Motion

Brownian motion can also be included in addititional force term in Equation 6. Brownian motion is a random motion of sub-micrometer particles inside a fluid which is caused by the geometrically unequal hit of the small fluid molecules on the particle surface. Usually, the Brownian motion is regarded as discovered by the botanist Robert Brown in 1827.

One computational scheme used to include Brownian motion into simulation was developed by Li. A and Ahmadi in 1993 [51]. In their work, the components of the Brownian force are modeled as a Gaussian white noise random process and the Brownian force is modeled as below:

$$F_{Br} = m_p G_i \sqrt{\frac{\pi S_0}{\Delta t}} \tag{9}$$

where m_p is the mass of the particle, G_i is unit variance zero mean Gaussian random

numbers obtained from a pair of random numbers N_1 and N_2 from the range [0, 1] and Δt is the time step used in the simulation to evaluate the amplitudes of the Brownian force. S_0 is given by:

$$S_0 = \frac{216 \nu k_B T}{\pi \rho d_p^5 \left(\frac{\rho_p}{\rho} \right)^2 C_c} \tag{10}$$

Where T is the absolute temperature of the fluid, ν is the kinematic viscosity of fluid, and k_B is the Boltzmann constant which is 1.38×10^{-23} J/K, other terms like C_C is the Cunningham correction and ρ is density.

- Saffman's Lift Force

The Saffman's lift force, or lift due to shear, can optionally be included in the additional force term. Lift force idea was first proposed by Saffman in 1965[52], after that Li and Ahmadi [51] proposed the expression for this force. In the particles balance equations, the Saffman's Lift Force term is defined as:

$$\vec{F} = \frac{2K\nu^{1/2}\rho d_{ij}}{\rho_p d_p (d_{lk} d_{kl})^{1/4}} \left(\vec{u} - \vec{u}_p \right) \tag{11}$$

Where d_{ij} is the deformation tensor, K is a constant K=2.594, and Re is the relative Reynolds number

1.4.2 Integration of Particle Motion Equation

Equation 6 can be integrated and an analytical expression of the particle velocity at next step u^{n+1} can be found in the form of:

$$u_p^{n+1} = e^{\frac{-\Delta t F_{drag}}{m_p}}\left(u_p^n - u^n\right) - \frac{m_p a_{total}}{F_{drag}}\left(e^{-\Delta t F_{drag}} - 1\right) + u^n \tag{12}$$

Here, the acceleration term a_{total} is the summation of all other accelerations except that caused by drag.

Remember the velocity of particle is defined as:

$$u_p = \frac{dx}{dt} \tag{13}$$

Equation 12 can be integrated again to obtain an analytical solution of the particle location at n+1 time step x^{n+1} :

$$x_p^{n+1} = \Delta t\left(u_n + \frac{m_p}{F_{drag}} a_{total}\right) + \frac{m_p}{F_{drag}}\left(1 - e^{-\frac{F_{drag}}{m_p}\Delta t}\right)\left(u_p^n - u^n - a_{total}\frac{m_p}{F_{drag}}\right) + x_p^n \tag{14}$$

Despite the analytical approach, the particle velocity and location can also be solved by using numerical discretization schemes such as trapezoidal discretization, Euler implicit discretization, and Runge-Kutta scheme [49].

1.5 Modeling the Drag Coefficients

The continuum phase can affect the discrete phase behavior though drag. There are two drag laws that may be useful in our simulation, one is spherical drag law and the other is the Stokes-Cunningham Drag Law.

The first one is the spherical drag law suggested by Morsi and Alexander in 1972. They studied the drag of particles in several different models, and finally derived an

empirical expression of the drag coefficient for smooth spherical particles in fluid described with different Reynolds Number from 0.1 to 50,000. In their studies, they used particles with diameter from 10 to 100 μm, and studied particles' response to one-dimensional flow, collision with a cylinder, and collision with a lifting airfoil. They claimed that the drag coefficients calculated from their equations are within 1-2% of experimental results. Their drag-Reynolds-Number relationship for spherical particles is shown in Eqn.15:

$$C_D = k_1 + \frac{k_2}{\mathrm{Re}} + \frac{k_3}{\mathrm{Re}^2} \tag{15}$$

Where Re is the Reynolds Number of the fluid, k_1, k_2 and k_3 are three empirical constants that may vary with Re. The values of these constants are listed below in Table below [49]:

Range of Reynolds Number Re	Expression of Drag Coefficient C_D
$Re < 0.1$	$24/Re$
$0.1 < Re < 1.0$	$22.73/Re + 0.0903/Re^2 + 3.69$
$1.0 < Re < 10.0$	$29.1667/Re - 3.8889/Re^2 + 1.222$
$10.0 < Re < 100.0$	$46.5/Re - 116.67/Re^2 + 0.6167$
$100.0 < Re < 1000.0$	$98.33/Re - 2778/Re^2 + 0{\cdot}3644$
$1000.0 < Re < 5000.0$	$148.62/Re - 4.75 \times 10^4/Re^2 + 0.357$
$5000.0 < Re < 10000.0$	$-490.546/Re + 57{\cdot}87 \times 10^4/Re^2 + 0.46$
$10000.0 < Re < 50000.0$	$-1662.5/Re + 5{\cdot}4167 \times 10^6/Re^2 + 0.5191$

The second drag law that may be valid is the Stokes-Cunningham Drag Law suggested by Ounis et al in 1991. They studied drag of particles with diameter from 0.01 to 0.1 μm, and showed that the Brownian effects play a significant role in the diffusion of submicrometer particles at distances less than 2 wall units from the solid surface. Expression for the drag acting on an individual particle is defined as:

$$F_D = \frac{18\mu}{d_p^2 \rho_p C_c} \tag{16}$$

Here F_D is the drag per unit particle mass and C_C is Cunningham correction to Stokes' drag law which can be obtain from Eqn.17:

$$C_c = 1 + \frac{2\lambda}{d_p}\left(1.257 + 0.4e^{-\frac{1.1 d_p}{2\lambda}}\right) \tag{17}$$

In this equation λ is molecular mean free path, which means the mean travel distance per collision, and can be calculated from Serway's approach:

$$\lambda = \frac{\bar{v}t}{\pi d_p^2 \bar{v} t n_v} = \frac{1}{\pi d_p^2 n_v} \tag{18}$$

Where n_V is the number of molecules per unit volume, *v* is the average velocity of the travelling molecule.

1.5.1 Specifying the Drag Function

A drag function for each pair of phases could be specified in ANSYS FLUENT. Below is the list of drag functions and their applications:

Boiling-ishii is to use the fluid-fluid drag function and this option is available when the boiling model is enabled.

Schiller-naumann is to use the fluid-fluid drag function. The Schiller and Naumann model is the default method, and it is acceptable for general use in all fluid-fluid multiphase calculations.

Morsi-alexander is to use the fluid-fluid drag. The Morsi and Alexander model is the most complete, adjusting the function definition frequently over a large range of Reynolds numbers, but calculations with this model may be less stable than with the other models.

Symmetric is to use the fluid-fluid drag function. The symmetric model is recommended for flows in which the secondary (dispersed) phase in one region of the domain becomes the primary (continuous) phase in another. For example, if air is injected into the bottom of a container filled halfway with water, the air is the dispersed phase in the bottom half of the container; in the top half of the container, the air is the continuous phase. The symmetric drag law is the default method for the Immiscible Fluid Model, which is available with Eulerian multiphase model.

Anisotropic is to use the fluid-fluid drag function described in Immiscible Fluid Model. The anisotropic drag law is recommended for free surface modeling. It is based on higher drag in the normal direction to the interface and lower drag in the tangenation direction to the interface. This is only available with Immiscible Fluid Model.

Universal-drag for bubble-liquid and/or droplet-gas flow when the characteristic

length of the flow domain is much greater than the averaged size of the particles. When universal-drag is selected, you will need to set a value for the surface tension coefficient, under the Surface Tension tab, in the Phase Interaction dialog box. This value will apply to the primary phase and the secondary phase.

Wen-yu is to use the fluid-solid drag function. The Wen and Yu model is applicable for dilute phase flows, in which the total secondary phase volume fraction is significantly lower than that of the primary phase.

Gidaspow is to use the fluid-solid drag function. The Gidaspow model is recommended for dense fluidized beds.

Syamlal-obrien is to use the fluid-solid drag function. The Syamlal-Obrien model is recommended for use in conjunction with the Syamlal-Obrien model for granular viscosity.

Syamlal-obrien-symmetric is to use the solid-solid drag function. The symmetric Syamlal-Obrien model is appropriate for a pair of solid phases.

Select constant to specify a constant value for the drag function, and then specify the value in the text field. If you want to temporarily ignore the interaction between two phases, select none.

1.6 Choosing the Spatial Discretization Scheme

The method of computing the gradient could be set in ANSYS FLUENT. Gradients are needed not only for constructing values of a scalar at the cell faces, but also for computing secondary diffusion terms and velocity derivatives.

The three gradients which are available in ANSYS FLUENT are

• Green-Gauss Cell Based

• Green-Gauss Node Based

• Least Squares Cell Based

Moreover, the discretization scheme for the convection terms of each governing equation could be choose in ANSYS FLUENT. Second-order accuracy is automatically used for the viscous terms. When the pressure-based solver is used, all equations are, by default, solved using the first-order upwind discretization for convection. When the density-based solver is used, the flow equations are solved using the second-order scheme by default, and the other equations use the first-order scheme by default.

1.7 Setting Under-Relaxation Factors

The interphase exchange of momentum, heat, and mass is under-relaxed during the calculation, so that

$$F_{new}=F_{old}+\alpha\ (F_{calculated}-F_{old})$$

$$Q_{new}=Q_{old}+\alpha\ (Q_{calculated}-Q_{old})$$

$$M_{new}=M_{old}+\alpha\ (M_{calculated}-M_{old})$$

where α is the under-relaxation factor for particles/droplets. The default value for α may be reduced to improve the stability of coupled calculations. Note that the value of does not influence the predictions obtained in the final converged solution.

The pressure-based solver uses under-relaxation of equations to control the update of computed variables at each iteration. This means that all equations solved using the pressure-based solver, including the non-coupled equations solved by the density-based solver, will have under-relaxation factors associated with them.

In ANSYS FLUENT, the default under-relaxation parameters for all variables are set to values that are near optimal for the largest possible number of cases. These values are suitable for many problems, but for some particularly nonlinear problems it is better to reduce the under-relaxation factors initially.

It is good practice to begin a calculation using the default under-relaxation factors. If the residuals continue to increase after the first 4 or 5 iterations, the under-relaxation factors should be reduced.

The default value of the under-relaxation factors in the Solution Controls task page are shown in figure 4.

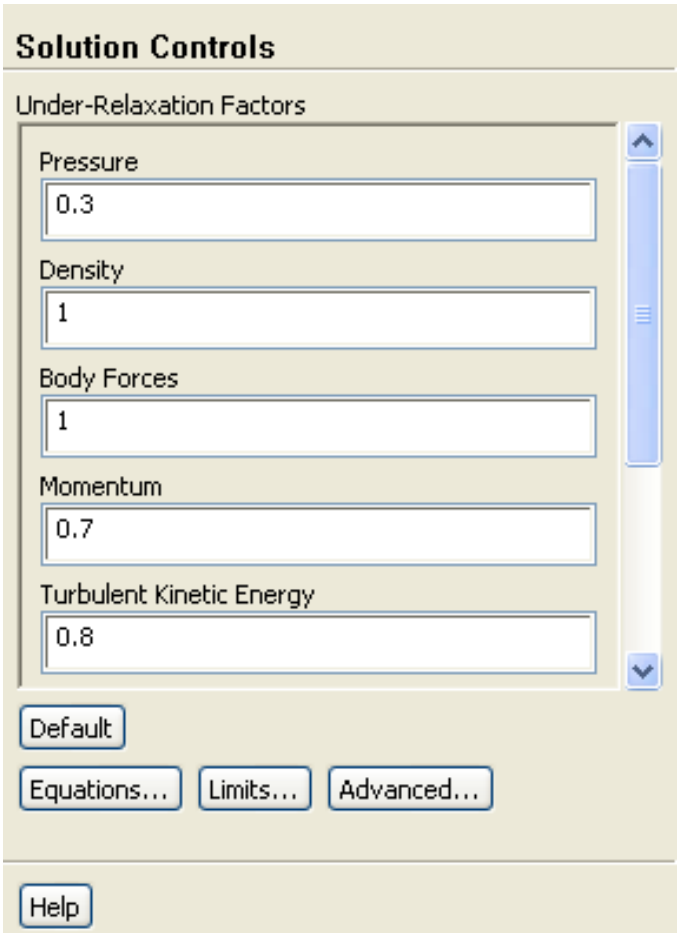

Figure 4. The Solution Controls Task Page for the Pressure-Based Solver

For most flows, the default under-relaxation factors do not usually require modification. If unstable or divergent behavior is observed, however, the under-relaxation factors for pressure, momentum, k, and ε should be reduced from their default values to about 0.2, 0.5, 0.5, and 0.5. (It is usually not necessary to reduce the pressure under-relaxation for SIMPLEC.) In problems where density is strongly coupled with temperature, as in very-high-Rayleigh-number natural- or mixed-convection flows, it is wise to also under- relax the temperature equation and/or density (i.e., use an under-relaxation factor less than 1.0). Conversely, when temperature is not coupled with the

momentum equations (or when it is weakly coupled), as in flows with constant density, the under-relaxation factor for temperature can be set to 1.0.

1.8 Choosing a Turbulence Model

The Viscous Model dialog box which is shown in figure 5 allows you to set parameters for inviscid, laminar, and turbulent flow.

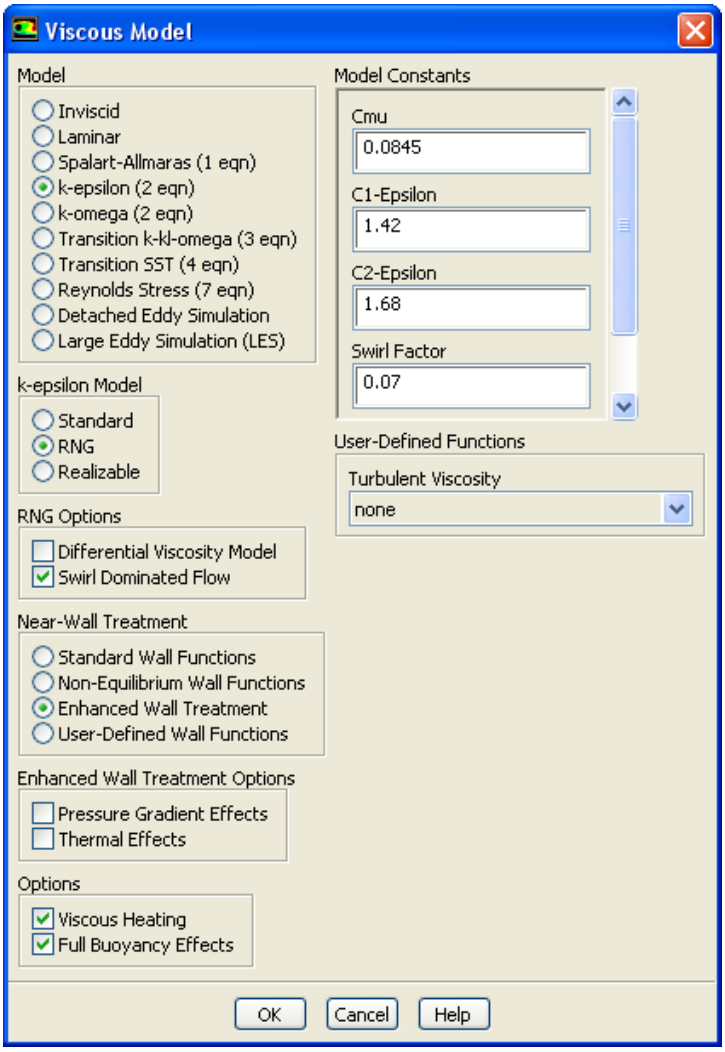

Figure 5. The Viscous Model Dialog Box Displaying the RNG k-ε Model

The models are as given in viscous model box is described below:

Inviscid: specifies inviscid flow. Inviscid flow analyses neglect the effect of viscosity on the flow and are appropriate for high-Reynolds- number applications where inertial forces tend to dominate viscous forces.

Laminar: specifies laminar flow.

Spalart-Allmaras: specifies turbulent flow to be calculated using the Spalart-Allmaras model. The Spalart-Allmaras model [53] is a one-equation model that solves a modeled transport equation for the kinematic eddy (turbulent) viscosity. The Spalart-Allmaras model was designed specifically for aerospace applications involving wall-bounded flows and has been shown to give good results for boundary layers subjected to adverse pressure gradients. It is also gaining popularity in turbomachinery applications.

In its original form, the Spalart-Allmaras model is effectively a low-Reynolds number model, requiring the viscosity-affected region of the boundary layer to be properly resolved. In ANSYS Fluent, the Spalart-Allmaras model has been extended with a insensitive wall treatment (Enhanced Wall Treatment), which allows the application of the model independent of the near wall resolution.

k-epsilon: specifies turbulent flow to be calculated using one of three k-ε models. (Standard, RNG, and Realizable k- ε)

All three models mentioned have similar forms, with transport equations for k and ε. The major differences in the models are as follows:

- The method of calculating turbulent viscosity
- The turbulent Prandtl numbers governing the turbulent diffusion of k and ε
- The generation and destruction terms in the ε equation

The standard k- ε model is a model based on model transport equations for the turbulence kinetic energy (k) and its dissipation rate (ε). The model transport for k is derived from the exact equation, while the model transport equation for ε was obtained using physical reasoning and bears little resemblance to its mathematically exact counterpart.

The RNG k-ε model was derived from the instantaneous Navier-Stokes equations, using a statistical technique (called renormalization group theory). The analytical derivation results in a model with constants different from those in the standard k-ε model, and additional terms and functions in the transport equations for k and ε. It is similar in form to the standard k -ε model, but includes the following refinements:

The RNG model has an additional term in its ε equation that improves the accuracy for rapidly strained flows.

The effect of swirl on turbulence is included in the RNG model, enhancing accuracy for swirling flows.

The RNG theory provides an analytical formula for turbulent Prandtl numbers, while the standard k-ε model uses user-specified, constant values.

While the standard k-ε model is a high-Reynolds-number model, the RNG theory provides an analytically-derived differential formula for effective viscosity that accounts

for low-Reynolds-number effects. Effective use of this feature does, however, depend on an appropriate treatment of the near-wall region.

These features make the RNG k-ε model more accurate and reliable for a wider class of flows than the standard k-ε model.

Transport Equations for the RNG k- ε Model are as given below:

$$\frac{\partial}{\partial t}(\rho k)+\frac{\partial}{\partial x_i}(\rho k u_i)=\frac{\partial}{\partial x_j}\left(a_k \mu_{eff}\frac{\partial k}{\partial x_j}\right)+G_k+G_b-\rho\varepsilon-Y_M+S_k \tag{19}$$

$$\frac{\partial}{\partial t}(\rho \varepsilon)+\frac{\partial}{\partial x_i}(\rho \varepsilon u_i)=\frac{\partial}{\partial x_j}\left(a_\varepsilon \mu_{eff}\frac{\partial \varepsilon}{\partial x_j}\right)+C_{1\varepsilon}\frac{\varepsilon}{k}(G_k+C_{3\varepsilon}G_b)-C_{2\varepsilon}\rho\frac{\varepsilon^2}{k}-R_\varepsilon+S_\varepsilon \tag{20}$$

In these equations, G_k represents the generation of turbulence kinetic energy due to the mean velocity gradients, calculated as described in Modeling Turbulent Production in the k- ε Models. G_b is the generation of turbulence kinetic energy due to buoyancy, calculated as described in Effects of Buoyancy on Turbulence in the k- ε Models. Ym represents the contribution of the fluctuating dilatation in compressible turbulence to the overall dissipation rate, calculated as described in Effects of Compressibility on Turbulence in the k- ε Models. The quantities α_k and α_ε are the inverse effective Prandtl numbers for k and ε, respectively. S_k and S_ε are user-defined source terms [49].

1.9 Initializing the Solution

Before starting CFD simulation, one must provide ANSYS FLUENT with an initial "guess" for the solution flow field. In some cases, you must be more careful to provide an initial solution that will allow the desired final solution to be attained.

Initialization method includes Hybrid Initialization and Standard Initialization.

- Hybrid Initialization is a collection of boundary interpolation methods, where variables, such as temperature, turbulence, species fractions, volume fractions, etc., are automatically patched based on domain averaged values or a particular interpolation recipe.
- Standard Initialization allows the user to define values for flow variables and initialize the flow field to these values. There are two methods for standard initialization: initialize the entire flow field (in all cells) or Patch values for selected flow variables in selected cell zones

1.10 Run calculation

According to the problem ANSYS FLUENT could solve the process by performing steady-state calculations or performing time dependent calculations. To solve the problem as steady state or time dependent, the steady or transient option should be enabled in general task page as shown in figure 6.

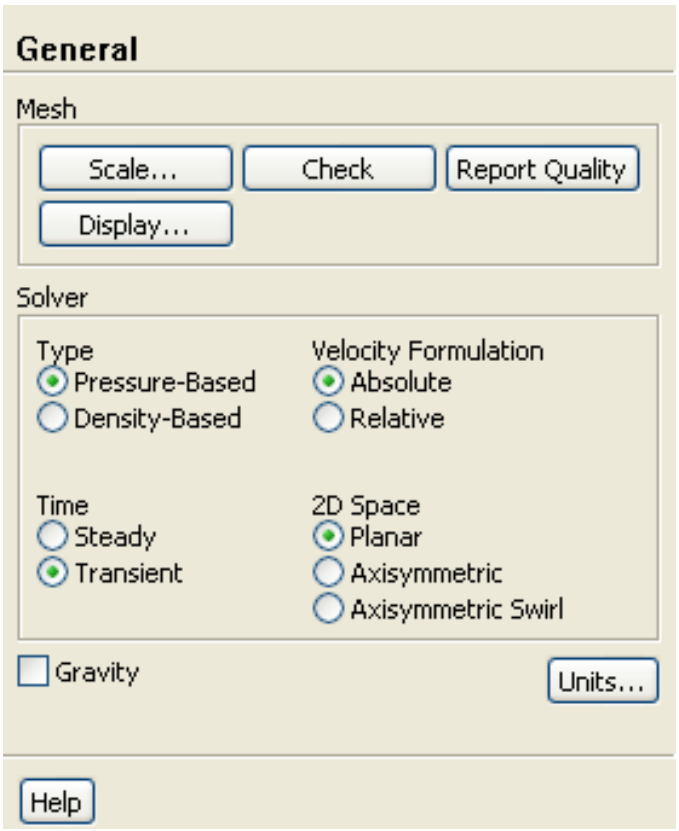

Figure 6.The General Task Page

1.10.1 Performing Steady-State Calculations

In this work we run the simulation in steady state. Here, the user will supply the number of iterations to be performed in the Number of Iterations field. If no calculations have been performed yet, ANSYS FLUENT will begin calculations starting at iteration 1, using the initial solution. If you are starting from current solution data, ANSYS FLUENT will begin at the last iteration performed, using the current solution data as its starting point. Figure 7 illustrates the Run Calculation task page for steady-state process.

By default, ANSYS FLUENT will update the convergence monitors after each iteration. By Increasing the Reporting Interval from the default (1) you can get reports less

frequently. For example, if you set the Reporting Interval to 2, the monitors will print or plot reports at every other iteration. Moreover, the Reporting Interval also specifies how often ANSYS FLUENT should check if the solution is converged. For example, if the solution converges after 40 iterations, but the Reporting Interval is set to 50, ANSYS FLUENT will continue the calculation for an extra10 iterations before checking for (and finding) convergence.

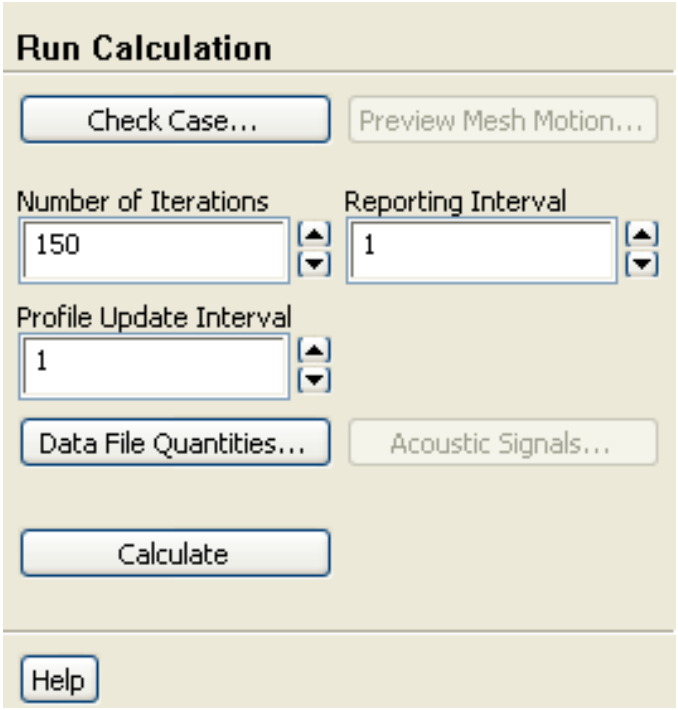

Figure 7. The Run Calculation Task Page for steady state process

1.10.2 Performing Time-Dependent Calculations

ANSYS FLUENT can also solve the conservation equations in a time-dependent manner. The first step to perform the simulation is to specify the desired Transient Formulation. The First Order Implicit formulation is sufficient for most problems, however, if improved accuracy is needed, the Second Order Implicit formulation could be used instead. The Explicit formulation (available only for the density-based solver) is used

primarily to capture the transient behavior of moving waves, such as shocks.

Solution parameters for the implicit transient formulations are as follows:

– Max Iterations/Time Step

– Time Step Size

– Time Stepping Method

During the solution process you the convergence can be monitored dynamically by checking residuals, statistics, force values, surface integrals, and volume integrals.

CURRICULUM VITA

NAME: Masoudeh Ahmadi

ADDRESS: 206A Ernst Hall
University of Louisville
Louisville, KY 40292

DOB: Tehran, Iran - May 26, 1984

EDUCATION & TRAINING:

B.S., Chemical Engineering, Kerman University, Kerman, 2004-2008

MSc. in Chemical Engineering Tehran Azad University, Tehran 2008-2010

Ph.D in Chemical Engineering University of Louisville, Louisville, KY 2011-2015

PUBLICATIONS:

Patents:

M. Ahmadi, P. Ratnasamy, M.A. Carreon, "Single-step process for production of branched, cyclic, aromatic, and cracked hydrocarbons from fatty acids," United States Patent Application No. 14/489,852, filed in September 2014

M. Ahmadi, P. Ratnasamy, M.A. Carreon, "Single-step decarboxylation and further conversion of fatty acids over bifunctional catalysts," United States Patent Application No. 61/948,139, filed in March 2014

Journal Publications:

M. Ahmadi, G. Willing, "Heat transfer enhancement in water-based CuO nanofluids," Under Review

M. Ahmadi, A.Nambo, J.B. Jasinski, P. Ratnasamy, M.A. Carreon, "Decarboxylation of oleic acid over Pt catalysts supported on small-pore zeolites and hydrotalcite," *Journal of Catalysis Science & Technology*, 2015,5, 380-3

M. Ahmadi, M.R. Ghasemi, H. Hashemipour, "Study of different parameters in TiO_2 nanoparticles formation," *Journal of Material Science and Engineering*, 2011, 5, 87-93

NATIONAL MEETING PRESENTATIONS

M. Ahmadi, G. Willing, "Measurement of Heat Transfer Mechanisms in Water-Based Nanofluids," *AIChE Annual Meeting*, Nov 2015, Salt Lake City, UT

M. Ahmadi, E.E. Macias, J.B. Jasinski, P. Ratnasamy, M.A. Carreon, "Oleic Acid Decarboxylation and Further Transformation over Pt/SAPO-11 catalysts and Pt/Al2O3 catalysts," *AIChE Annual Meeting*, Nov 2014, Atlanta, GA

M. Ahmadi, A. Nambo, J.B. Jasinski, P. Ratnasamy, M.A. Carreon, "Decarboxylation and further isomerization of oleic acid over Pt-supported on small pore zeolites and hydrotalcite catalysts," *AIChE Annual Meeting*, Nov 2014, Atlanta, GA

M. Ahmadi, J. Jasinski, M. Carreon, "Decarboxylation of oleic acid over solid catalysts," *North American Catalysis Society Meeting*, June 2013, Louisville, KY

M. Ahmadi, M.R. Ghasemi, H. Hashemipour, "Investigating of operating conditions effects on TiO2 nanoparticles properties," *International Conference on Nanoscience and Nanotechnology*, February 2010, India